
Article:
Celik, Y., Ma, L., Ingham, D. et al. (1 more author) (2020) Aerodynamic investigation of the start-up process of H-type vertical axis wind turbines using CFD. Journal of Wind Engineering and Industrial Aerodynamics, 204. 104252. ISSN 0167-6105

https://doi.org/10.1016/j.jweia.2020.104252

Aerodynamic investigation of the start-up process of H-type vertical axis wind turbines using CFD

Yunus Celik[a], Lin Ma[a*], Derek Ingham[a], Mohamed Pourkashanian[a]

[a] *Energy2050, Department of Mechanical Engineering, Faculty of Engineering, University of Sheffield, Sheffield, UK*

Abstract

In this study, a CFD start-up model has been built after conducting the sensitivity studies to evaluate the self-starting behaviour of the H-type vertical axis wind turbines (VAWTs). The self-starting behaviour of a well-investigated VAWT is used for the model validation, and then the details of aerodynamics of the start-up process have been examined. Finally, the effect of the moment of inertia and the blade number on the aerodynamic behaviour of the self-starting and power performance of the H-type VAWT are analysed. It has been found that in the critical region, where TSR<1, the contribution of the drag to the torque generation plays a significant role in the second and third quarters of the rotor revolution, where the azimuthal position varies between 100° and 253°. The results also show that increasing the turbine inertia did not show a noticeable effect on the start-up behaviour of the turbine and final rotational speed. However, an increase in the instantaneous turbine power during the start-up process after the optimum TSR is observed with decreasing the turbine inertia. The current findings also show that an increase in the blade number makes the turbine easier to start-up; however, this may reduce the turbine power coefficient.

Keywords

Self-starting, Vertical axis wind turbine, Aerodynamics, CFD, Moment of Inertia, Blade number

* Corresponding author. The University of Sheffield, Department of Mechanical Engineering, Faculty of Engineering, University of Sheffield, Sheffield, UK.

E-mail address: lin.ma@sheffield.ac.uk

1. Introduction

As a result of human activities, such as the burning of fossil fuels, the greenhouse gases in the atmosphere have been increasing, and this causes climate change (Kose and Kaya, 2013). For this reason, the demand for renewable energy sources has increased. Renewable energy offers our planet a chance to decrease carbon emissions, make the environment cleaner, and put our civilisation on a more sustainable footing (Juneja et al., 2012). Renewable energy sources can be categorised as wind energy, solar energy, hydrogen energy, biomass and hydro. Among the renewable energy sources, wind energy has grown rapidly and will play an increasingly crucial role in the future economy.

The wind is a natural alternative energy resource and generally employed by the wind turbines in order to generate electricity. There are generally two different types of wind turbines, such as horizontal axis wind turbines (HAWTs) and vertical axis wind turbines (VAWTs). Furthermore, VAWTs have two different types, namely, the Savonius type, which is a drag-based turbine, and the Darrieus type, which is a lift-based turbine. The Darrieus wind turbines are divided into two groups due to their shapes, which are the eggbeater and H-type turbine, which is also known as a straight-bladed vertical axis turbine (SB-VAWT) (Almohammadi, 2014). In these days, HAWTs have dominated the wind energy market due to their large size and high power generation capacity (Kaya et al., 2018). However, the advantages of VAWTs have been recently emphasized (e.g. Edwards et al., 2012; Bertényi et al., 2010), these being such as being more suitable for urban environmental applications than the more commonly adopted HAWTs due to several significant advantages, such as affordable maintenance cost, simple blade shape, omni-directional work capability and low noise (Almohammadi, 2014).

Even though VAWTs still suffer from low efficiency compared to conventional HAWTs, one of the most challenging aspects of these types of the turbine is the ability of the self-start. Although the external power sources are generally used to start-up the turbine, the need for the turbine assistance to start brings extra complexity and energy expense (Bos, 2012). Therefore, in order to address this challenge, several solutions have been proposed such as the Hybrid turbine designs (Bhuyan and Biswas, 2014; Hosseini and Goudarzi, 2019; Liu et al., 2019) which consist of the Darrieus and Savonius wind turbines, and the active/passive pitching mechanism design (Nahas, 1993). However, the major problem with these kinds of solutions is that the power performance of the turbine is decreased while the self-starting capability is enhanced.

In this paper, an H-type Darrieus VAWT is studied in terms of the aerodynamic characteristics of the start-up using a CFD method, and investigating the effects of the physical properties, such as inertia and the number of blades on its self-starting behaviour and power performance by using the dynamic start-up model instead of employing several constant rotational speeds of the turbine. The overall aim

is to improve the understanding of the self-starting process and set a basis for future analysis and optimisation.

2. Self-starting and current studies

There are several types of definitions of self-starting. Even though they have a similar meaning, the way of explaining it is different. The self-starting was described by Ebert and Wood (1997) as the self-starting process is completed when the significant power extraction begins. At the same moment, Kirke (1988) introduced a comparable definition that considers a turbine to be self-starting only if it can accelerate from rest to the stage where it can begin producing useful energy output. If we look at these two definitions, it can be understood that the meaning that the terms' significant power' and 'useful output' are themselves imprecise. A more specific definition of the self-starting has been adopted by Lunt (2005). He claims that the self-starting occurs only if the turbine accelerates from the rest to the steady-state condition, where turbine speeds exceed the free wind speed (TSR>1). Under these circumstances, the positive drag contribution to the torque generation can no longer be existing while a significant lift is generated in a complete revolution. Even though this definition is more precise, it also has its limitations as it does not guarantee that the turbine will continue to accelerate when it reaches a point where it starts to produce a significant lift in a complete revolution. In this paper, the turbine is considered to be self-starting only if it accelerates from rest to its final operating tip speed ratio, where the turbine has already passed the plateau stage, without any need of the external power.

Many researchers have focused on the self-starting of the vertical axis wind turbines by using different methods. Untaroiu et al. (2011) replicated an experimental prototype by employing 2D and 3D CFD models of a three-bladed vertical axis wind turbine. In addition, the authors have conducted sensitivity studies in terms of the time step size and inlet turbulence intensity. The results show that a 0.001s time step size is found to be sufficient to operate the turbine until the steady-state condition has been achieved. Furthermore, they have found that even though 2D transient CFD simulations can predict the turbine operating speed with a 12% error, the 2D CFD simulations when compared to the 3D CFD simulations do not accurately capture the performance of the turbine. This is due to the generation of tip vortices from the 3D model, which do not appear in 2D, and this considerably reduces the speed of the rotating blades of the turbine. In addition, the SST k–ω turbulence model has been recommended by the authors. Beri and Yao (2011) have investigated the effect of the modified airfoil trailing edge on the self-starting behaviour of the vertical axis wind turbines at low tip speed ratios using the CFD method. The results indicate that the modified airfoil had a better self-starting performance than the cambered airfoil due to the higher moment coefficient for all the azimuthal angles. Worasinchai et al. (2012) have created a Blade Element Momentum (BEM) model based-model in order to evaluate the self-starting behaviour of the VAWT. In addition, the authors investigated the

flow physics of the flapping-wing mechanism and its relation to the Darrieus turbine blade. According to the conclusion, the flapping analogy suggests that the symmetrical airfoil with a careful configuration of the chord-to-diameter ratio, blade aspect ratio, and the number of blades may increase the driving torque generation and the ability of the self-start. Rossetti and Pavesi (2013) compared the BEM model with 2D and 3D CFD models. In order to assess the self-starting behaviour, the tip speed ratio as a function of the power coefficient curve and thrust force over a blade revolution have been highlighted. According to the authors' conclusion, the BEM model indicates a remarkable limit in the describing of the self-starting due to the absence of the data in the literature for the lift and drag coefficients of the airfoil for the low Reynolds number and the inappropriate modelling of the dynamic stall. In addition to this, the difference between the 2D and 3D CFD results are due to the secondary flows, exclusion of the three-dimensional effects, such as blade tip losses, and finite aspect ratio of the blades. Bhuyan and Biswas (2014) experimentally studied the self-starting behaviour and performance characteristics of the simple H-type and Hybrid H-Savonius vertical axis wind turbines. The results show that the hybrid turbine design increases the self-starting capability due to the positive torque coefficient values at all azimuthal angles.

Zhu et al. (2015) provided a systematic of the fluid-turbine interaction process in terms of the self-starting behaviour of the H-type VAWT based on CFD. Once the model has been obtained, then the effect of the solidity and fixed pitch angle on the self-starting behaviour have been investigated. According to the results, the solidity is not able to make the turbine have a fast self-starting and high power performance, simultaneously. However, a -2.5° fixed pitch angle can make the turbine have both a faster self-starting time and a larger power coefficient. Singh et al. (2015) conducted an experimental investigation of the self-starting behaviour and high rotor solidity on the performance of a three S1210 blades H-type Darrieus rotor. The results show that the asymmetrical airfoil with increased rotor solidity can be chosen in order to produce a potential solution for the self-starting problem. Sengupta et al. (2016) investigated symmetrical and cambered airfoils with high solidity in terms of self-starting behaviour of the H-type VAWT. In this study, two cambered airfoils, namely S815 and EN0005 and one symmetrical NACA0018 airfoil, have been examined for both numerical and experimental investigations. It has been found that the turbine with an asymmetrical E815 airfoil has a higher dynamic torque and higher power coefficient than other airfoils. Zhu et al. (2016) numerically analysed the self-starting aerodynamic characteristics of the vertical axis wind turbine under fluctuating wind conditions. They have found that if the fluctuating wind with appropriate fluctuation amplitude and frequency is determined, the capability of the self-starting behaviour of the VAWT could be improved.

Torabi et al. (2016) studied the self-starting behaviour of the VAWT by using an appropriate CFD modelling setup. In contrast to the conventional approach, the turbine starts to accelerate based on the

torque experienced over time. A sensitivity study has been carried out in order to determine the domain size, yielding the distances of 4r and 10r from the centre of the turbine to the domain inlet and outlet, respectively. Furthermore, symmetrical and asymmetrical airfoils of various thicknesses with a wide range of pitch angles have been investigated with the validated CFD model. The results showed that the asymmetrical airfoil NACA2418, with the positive pitch angle of 1.5 degrees, shows a significant enhancement in the rotor acceleration as 27% faster speed-up. Douak et al. (2018) has been conducted the numerical and experimental studies in order to evaluate the self-starting capability of the optimised H-type VAWT. The results indicated that the optimal angle of attack in order to obtain a maximum torque is AoA=15°. They claim that this angle increases the capability of the self-starting at low wind speeds conditions, and the three-bladed turbine has the self-starting capability, regardless of the starting position of the turbine. Hosseini and Goudarzi (2019) aimed to design, simulate and investigate the performance of the hybrid vertical axis wind turbine in order to increase the self-starting capability and operational range of the turbine. In this study, two-bladed Savonius Bach-type turbine and three-bladed H-type VAWT have been used to design a hybrid turbine by using the CFD method. The results show that the self-starting capability of the turbine has been increased with a maximum power coefficient of 0.414 at a TSR of 2.5 and the operational range was extended up to TSR of 4.5. A summary of the studies related to the self-starting behaviour of the VAWT has been presented in Table 1.

Table 1. Summary of the self-starting studies.

Authors	Year	Scope of the study	Limitations
Untaroiu et al. (Untaroiu et al., 2011)	2011	2D and 3D start-up model.	Accuracy of the turbulence model selection.
Beri and Yao (Beri and Yao, 2011)	2011	The effect of modified airfoil trailing edge on the self-starting behaviour.	The self-staring behaviour of the turbine has been assessed with the constant angular velocities. However, a dynamic start-up simulation is required.
Worasinchai et al. (Worasinchai et al., 2012)	2012	BEM based self-starting model.	Absence of the aerodynamic data for the lift and drag coefficients at low Reynolds numbers.

Rossetti and Pavesi (Rossetti and Pavesi, 2013)	2013	BEM based self-starting model with modified aerodynamic data.	The limitation of the BEM model due to the lack of accuracy of the aerodynamic data for lift and drag coefficients and inappropriate modelling of the dynamic stall.
Bhuyan and Biswas (Bhuyan and Biswas, 2014)	2014	Hybrid turbine design.	Turbine self-starting characteristics has been evaluated based on the turbine torque coefficient versus azimuthal angle. The dynamic start-up simulation is required to ensure the turbine completely self-starts.
Zhu et al. (Zhu et al., 2015)	2015	Investigation of the solidity and fixed pitch angle based on the CFD model.	Lack of the detail of the CFD model in the sensitivity study. In addition, the effect of the number of blades is not considered when the solidity was examined.
Singh et al. (Singh et al., 2015)	2015	Experimental study of the turbine self-starting considering the airfoil type and turbine solidity.	The aerodynamics of the other unsymmetrical blade H-Darrieus turbines with high solidity should be investigated.
Zhu et al. (Zhu et al., 2016)	2016	Fluctuating wind condition has been examined in terms of the self-starting characteristics of the VAWT.	The results obtained appear to indicate that the findings are valid for only some selected free streams. To generalize this finding, other wind speed conditions should be investigated.
Torabi et al. (Torabi et al., 2016)	2016	Investigation of different types of blade and pitch angle based on the CFD model.	The results obtained are valid for the specified wind speed condition. These could be generalized.
Hosseini and Goudarzi (Hosseini and Goudarzi, 2019)	2019	Hybrid turbine design.	Even though the hybrid design generates high initial torque, it is not guarantee that the turbine could escape the plateau stage to reach the steady state position.

The literature survey shows that there are a considerable number of studies on the self-starting characteristics of the VAWTs by employing different methods, such as the Computational Fluid Dynamics model (CFD) and Blade Element Momentum model (BEM). One of the main drawbacks of

the BEM method is the accuracy of the results due to the absence of the data in the literature for the lift and drag coefficients at low Reynolds numbers. On the other hand, some of the previous CFD studies have not produced an accurate model for evaluating the self-starting behaviour of the turbine. It is believed that one of the reasons for the inaccurate results with the CFD method may be due to the lack of a careful investigation of the effects of the domain size, mesh generation, the time step size, and turbulence models. On the other hand, several studies have been conducted to investigate the effect of the physical parameters, such as solidity, pitch angle, blade profile, etc., on the self-starting behaviour with the calculated instantaneous torque and power coefficients at low tip speed ratios (e.g. TSR<1). However, little attention has been paid to the turbine time-varying start-up data together with the overall power performance data obtained from the dynamic start-up simulations, especially in terms of the effects of the turbine moment of inertia and the number of blades on the self-starting. The effect of turbine inertia on the starting time and in particular on the torque/power generation during acceleration phase have been observed for the first time.

According to the above discussions, one of the main aims of the present study is to enhance the knowledge of how vertical axis wind turbines can gain self-starting characteristics by a detailed investigation of the start-up process, aerodynamically. A Computational Fluid Dynamic (CFD) start-up model technique has been built with own user defined function (UDF) after conducting sensitivity studies, such as domain size, time step size, and the number of nodes around the airfoil to obtain an accurate CFD model. Once an accurate model has been obtained, the output results have been compared with experimental data. With the validated CFD model, a detailed aerodynamic investigation of the start-up process of the H-type VAWT was performed. Furthermore, the contributions of the aerodynamic lift and drag of the turbine blade at various azimuthal positions to the turbine starting up have been analysis in great detail which should provide important insights on optimizing an VAWT design. Then, the effects of the moment of inertia and the blade number on the aerodynamic behaviour of the self-starting and turbine performance of the H-type VAWT are analysed using the dynamic start-up model instead of employing several constant rotational speeds to the turbine.

3. CFD modelling and validation

3.1. Simulation parameters and turbulence modelling

There are few experimental studies available in the literature in terms of the turbine self-starting. For this reason, a published experimental data, carried out by Rainbird (2007) has been selected in order to validate the CFD start-up model. One advantage of the selected experimental study is that it allows for a direct comparison of the turbine self-starting behaviour rather than only the calculated torque and power coefficients. Furthermore, in the experimental study, a ¾ open jet design wind tunnel, which eliminates the sidewall interference, has been used since open jet tunnels are much less sensitive to the

blockage than the closed wall tunnels. However, the uncertainties in the measurements have not been mentioned in the experiment.

In this study, the geometry of the investigated VAWT has been created based on the setup of the experiment by Rainbird (2007). The turbine is constructed of three NACA0018 airfoils with a chord length of 0.083 m. The ANSYS Design Modeller has been used to create the CFD model, and Table 2 summarised the main characteristics of the wind turbine.

Table 2
Turbine Configurations.

Name	Value	Unit
Blade Profile	Naca0018	-
Number of blades	3	-
Span height	0.6	m
Chord length	0.083	m
Radius	0.375	m
Rotor moment of inertia	0.3	kgm²

A pressure-based solver, which is SIMPLE, with gradient called Green-Gauss Node Based, was applied. The second-order upwind scheme is used for the spatial discretisation of the pressure, the turbulence model and the momentum equations. In order to assess the sensitivity of the results in terms of the number of iteration and residual convergence criteria, the simulations have been run using different numbers of iterations and the magnitude of the convergence criteria. The results show that each time step requires at least 25 iterations to reduce each residual convergence criteria to five orders of the magnitudes, and this finding is in agreement with Wekesa et al., (2016). Turbulent intensity is unknown in the experimental study; therefore, a sensitivity analysis has been conducted in order to define the turbulent intensity and viscous ratio, and these have been chosen as 1% and 10, respectively.

In the conventional approach of the CFD simulations, several constant rotational speeds are defined for the rotor, and the torque is calculated for each rotational speed by neglecting the turbine moment of inertia. However, in this study, the variation in the turbine rotational speed, which is driven by the wind, is calculated based on the torque generation at each time step. For this purpose, the 6DOF, which includes the physical characteristics of the turbine and its moment of inertia, has been written in the C language and linked to the ANSYS Fluent solver under the dynamic mesh zone section. In addition to this, only one degree of freedom, which rotates around the turbine axis, has been taken into account. In the experimental setup, the turbine moment of inertia has been stated as 0.018 kgm^2; however, in the 2D CFD simulation, the moment of inertia is calculated as 0.03 kgm^2 depends on the per unit span, and the predicted result is consistent with Zhu et al. (2015). All simulations have been performed on

the HPC (High-Performance Computing) facilities provided by the University of Sheffield and when 16 cores were used, the time spent on each simulation was at least 7 hours.

Selecting the turbulence model plays a significant role, especially at the low TSRs due to the complex flow structures of the VAWT. In the literature, the two-equation turbulence models, such as k–ε and k–ω, are commonly used for the simulations. Three different types of k–ε models are available for turbulent flow simulations such as the standard, the RNG, and the Realizable k–ε models, which have similar forms with transport equations for k and ε (Song et al., 2015). The significant difference between these models is the method for the calculation of the turbulence viscosity and the generation and the destruction terms in the ε equation. On the other hand, a two-equation eddy-viscosity turbulence model, which is SST k–ω, has become very popular. In order to make the model directly applicable in the viscous sub-layer, k–ω formulation in the inner parts of the boundary layer is employed. Therefore, the SST k–ω model can be applied as a low-Reynolds turbulence model without any additional damping functions (D'Alencon and Silva-Llanca, 2016). The SST k–ω model is a combination of the k–ω and k–ε models. In the inner part of the boundary layer, the k–ω model is used and the k–ω model is gradually switched to the standard k–ε behaviour in the free-stream in order to eliminate the inaccuracy of the k–ω in the boundary layer (Menter, 1994). In this context, the SST k–ω turbulence model has been preferred in many CFD simulations and validated experimentally by researchers (Torabi et al., 2016; Menter, 2009; Langtry et al., 2006; Menter et al., 2005; Balduzzi et al., 2016; Castelli et al., 2010; Bedon et al., 2015; Nobile et al., 2014). Therefore, the SST k–ω turbulence model is employed in the present study.

3.2. Model sensitivity studies

3.2.1 Domain size study

The computational domain is decomposed into a rotational domain, which contains the rotor, and a fixed rectangular outer domain in order to provide the conservation of both mass and momentum during the simulation. The two regions are connected using interface boundary conditions to ensure that the continuity in the flow field is established. The velocity inlet is applied to the left side of the computational domain with a constant velocity profile of 6 m/s, and this value is selected according to the experimental conditions of Rainbird (2007). A zero gauge pressure outlet is imposed on the right side of the computational domain, and the blade surfaces are considered as no-slip boundaries. Two symmetry boundary conditions were implemented at the top and bottom sides of the computational domain in order to reduce the impact of the solid blockage effects (Nobile et al., 2014). A schematic of the domain created for the computations is shown in Fig. 1. As indicated in the figure, A is the distance between the velocity inlet and the centre of the turbine, B is the distance between the centre of the

turbine and the pressure outlet, C is the distance between two symmetry boundaries, D is the radius of the circular subdomain that is associated with region of the turbine, and E is the radius of the small circular subdomains that are located at the vicinity of the blades to increase the mesh intensity in these regions. In order to perform a sensitivity study to determine the required computational domain size, three different cases, namely Domain 1, Domain 2 and Domain 3, have been investigated, and the values of each case are shown in Table 3. The values for the Domain 1 have been selected according to Zhang et al. (2013), and then these values have been proportionally increased for Domain 2 and Domain 3 to find optimum values for the computational domain. The domain size independent study has been conducted at a relatively small tip speed ratio of 1.5 and at a tip speed ratio of 3 in order to ensure that the results do not show any discrepancies at these two different tip speed ratios.

Table 3
Computational domain sizes for validation study.

Name	Values				
	A	**B**	**C**	**D**	**E**
Domain 1	6r	24r	12r	2r	0.5r
Domain 2	8r	32r	16r	2.5r	1r
Domain 3	10r	40r	20r	3r	1.5r

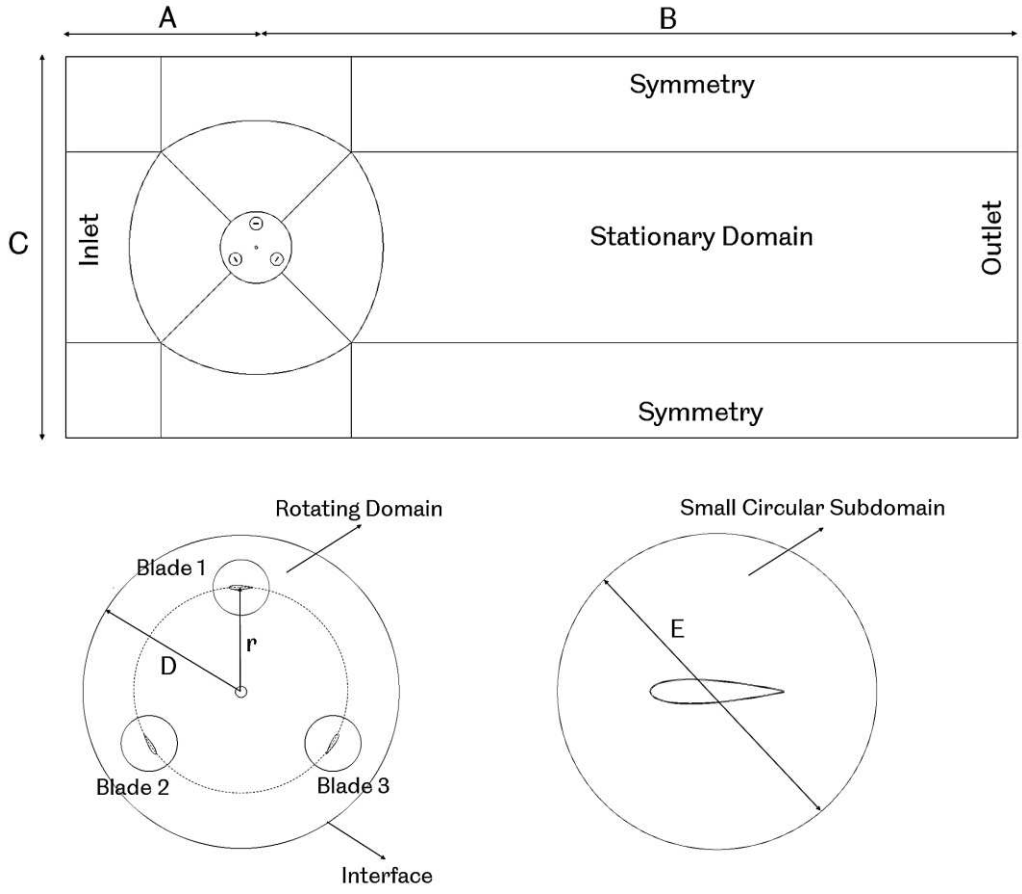

Fig. 1. Schematic of the domain created for the computations.

The blade moment coefficient as a function of the azimuthal angle for both the tip speed ratio is plotted in Fig. 2, and it is observed that the results for the Domain 2 matches closely to that of Domain 3 for both TSRs while the result for the Domain 1 is different. Therefore, Domain 2, which has the dimensions of 40r and 16r in the directions parallel and perpendicular to the free stream velocity, respectively, has been chosen for the further self-starting simulations of VAWT in this paper. Furthermore, using the computational domain with 32R distance from the turbine centre to the domain outlet is determined to be a safe choice in order for the domain to be sufficiently large so that the wake fully develops inside the computational domain, and this is consistent with other relevant studies. (Posa, 2020; Li et al., 2017; Rezaeiha et al., 2017).

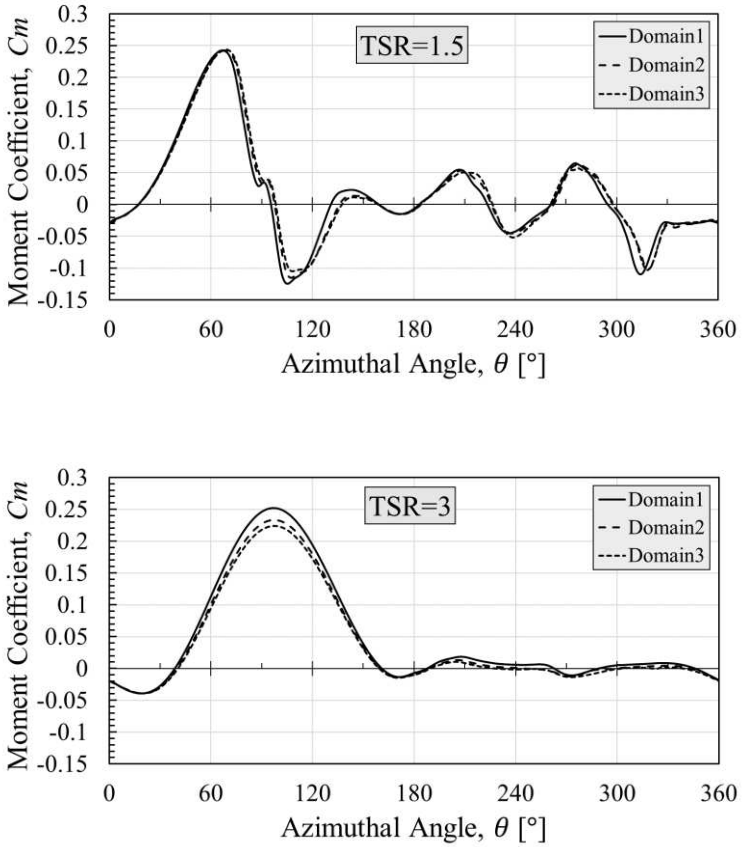

Fig. 2. The moment coefficient as a function of the azimuthal angle for the domain size study at TSR=1.5 and TSR=3.

3.2.2. Grid topology

One of the most critical parts of the CFD simulations is the mesh generation due to its impact on the accuracy of the model. The behaviour of the flow within the boundary layer is a complicated phenomenon. Therefore, in order to define the order of the magnitude for the size of the cells in the boundary layer region, the dimensionless wall distance, namely y^+, should be determined according to the turbulence model (ANSYS, 2014). In order to allow the turbulence model to predict the

performance, the literature recommends that the boundary layer with at least 10 layers of cells should be employed (ANSYS, 2013). In the present study, 15 mesh layers with the first cell height of about 2×10^{-5}m have been used in order to obtain a y^+ value with a maximum wall distance 2.5 and average $y^+ < 1$. By maintaining these values, a proper estimation of the aerodynamic forces in the boundary layer can be achieved (Elsakka et al., 2019; Sun et al., 2020).

A hybrid mesh is chosen as the most appropriate mesh type in this study since the hybrid mesh provides a flexible approach and reduce the number of mesh elements in the computational domain. As it can be seen from the Fig. 3, the hybrid mesh consists of a structured mesh employed for both around the airfoil and in the far field, while an unstructured mesh is employed for the rotating domain.

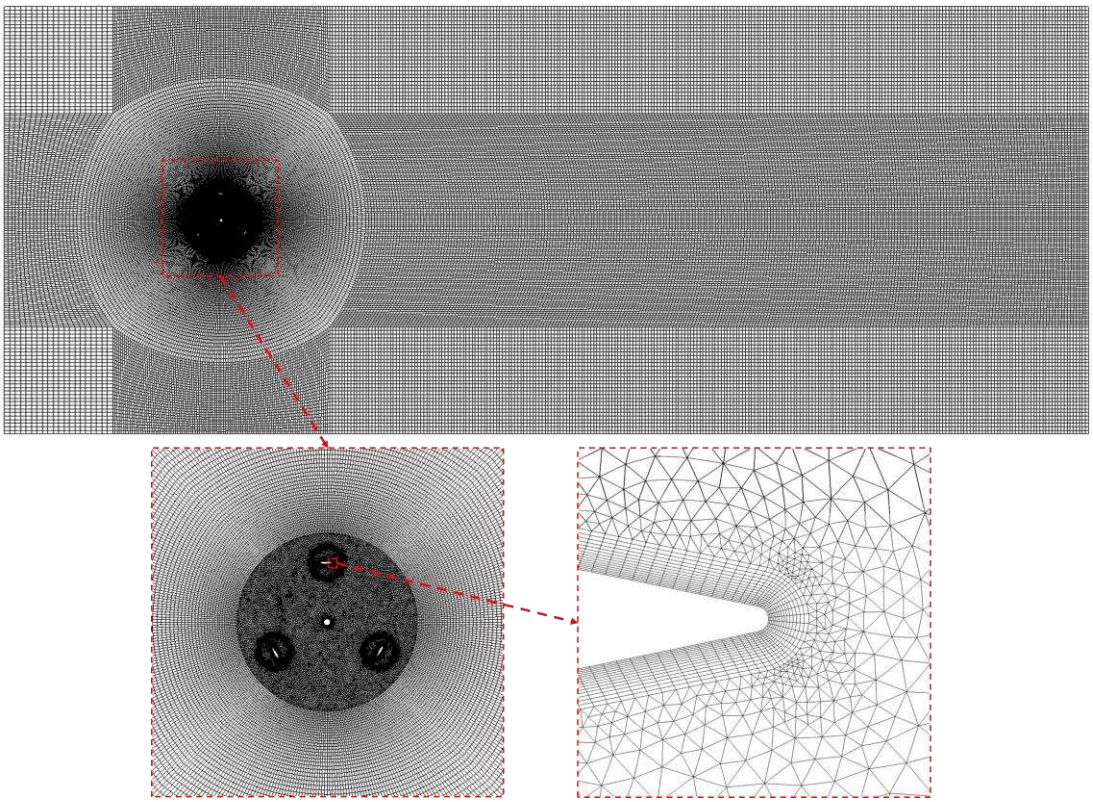

Fig. 3. Grid configurations for the whole domain, the rotating domain and at the vicinity of the blade.

Three different number of nodes, as illustrated in Table 4, have been investigated in order to obtain an optimal number of nodes around the airfoil at two different TSRs. For this purpose, Nodes 1, 2, and 3, which have 800, 1000, and 1200 nodes, respectively, have been created by using the ANSYS Meshing Module. The grid sensitivity study was performed based on these three sets of nodes around the airfoil. The Grid Convergence Index (GCI) (Roache, 1997) was calculated based on the 2D turbine power coefficient using a safety factor 1.25 (Rezaeiha et al., 2018a) for both tip speed ratios (TSR=1.5 and TSR=3). The $\mathrm{GCI}_{\mathrm{fine}}$ for the Node 2-Node 3 pair are found to be about 1.2×10^{-3} and 2.2×10^{-3}

for TSR=1.5 and TSR=3, respectively and this corresponds to about 1.56% and 0.6% of the 2D turbine power coefficient, respectively. Furthermore, a comparison of the results on the moment coefficients as a function of the blade azimuthal angle for the different number of nodes at the two TSRs are presented in Fig. 4. As can be seen from the figures, there is a negligible difference in the moment coefficients over all azimuthal angles between Nodes 2 and 3 at both tip speed ratios while Node 1 is different. Therefore, the most reasonably accurate and computationally economic number of nodes are found to be 1000 at both TSRs and chosen for the further self-starting simulations of the VAWT in this study. The mesh having 127,000 elements in the rotating domain and 77,000 elements in the fixed domain has been created after the sensitivity study was performed.

Table 4
The number of nodes around the investigated airfoil.

	Values		
	Node 1	**Node 2**	**Node 3**
Number of Nodes	800	1000	1200

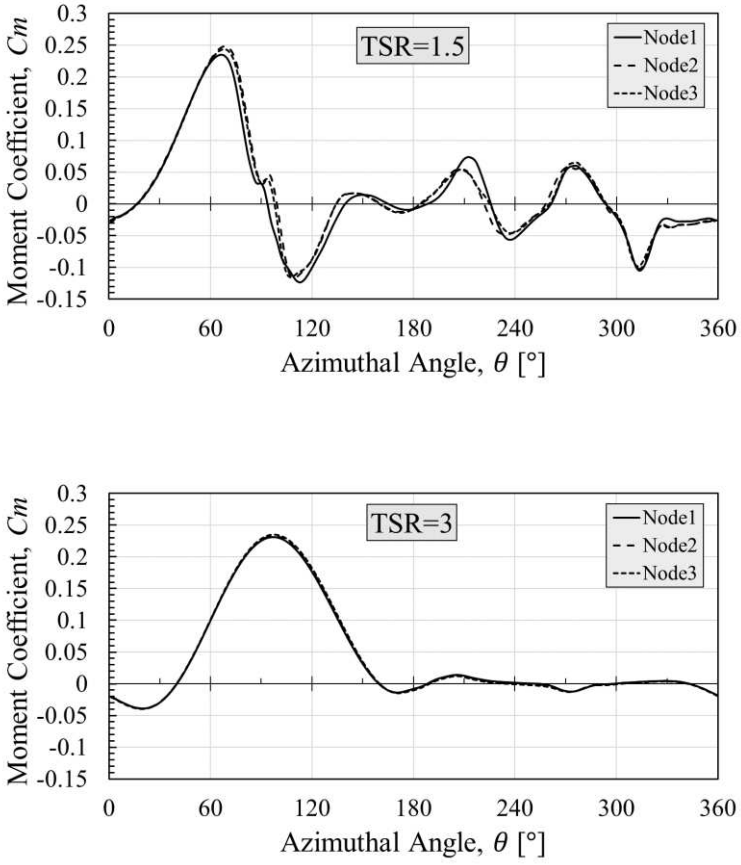

Fig. 4. The moment coefficient as a function of azimuthal angle for the nodes study at TSR=1.5 and TSR=3.

3.2.3. Time step size study

For the time step size study, three time steps, which are $\Delta t1$ =0.00144s, $\Delta t2$ =0.00072s, and $\Delta t3$ =0.00036s, have been examined in order to evaluate the impact on the results concerning the length of time steps. According to the results, which are shown in Fig. 5, there is only a slight difference between $\Delta t2$ and $\Delta t3$ with the identical trend in the moment coefficient at both tip speed ratios. Therefore, $\Delta t2$ is selected for further simulations to reduce the computational time. The selected time step size, which is 0.00072s, is consistent with other researches. (Torabi et al., 2016; Untaroiu et al., 2011).

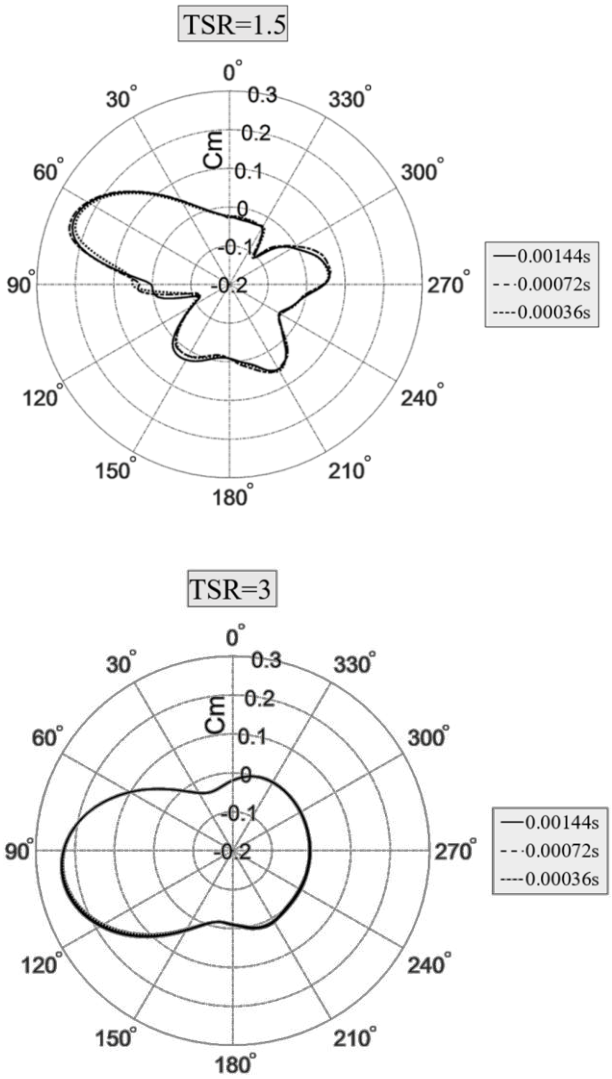

Fig. 5. The moment coefficient as a function of azimuthal angle for the time step size study at TSR=1.5 and TSR=3.

It is important to note that in all the verification studies, namely the domain size, number of nodes around the airfoil, and the time step size, the moment coefficients are calculated at the 20th revolution in order to reach the statically steady state condition for both tip speed ratios investigated. This number

of revolutions is sufficient and consistent with the published guideless for the CFD simulations of the VAWTs (Rezaeiha et al., 2018a).

3.3. Model validation

Fig. 6 shows a comparison between the current CFD prediction with the experimental data obtained by Rainbird (2007). It can be seen from the figure that the current CFD model is able to predict the self-starting behaviour of the turbine. However, to make it easier to understand the comparison between the experimental and the current numerical results, the non-dimensional time axis, which is defined as t/T (T is the time when the steady-state condition is reached) is employed. The time required to reach steady-state condition is about 150 seconds in the experiment while it is about 15 seconds in the current CFD study. The finding of the current study is consistent with those of Untaroiu et al. (2011), Zhu et al. (2015), and Torabi et al. (2016) who found the start-up time as about 18 seconds, 10 seconds, and 12 seconds, respectively.

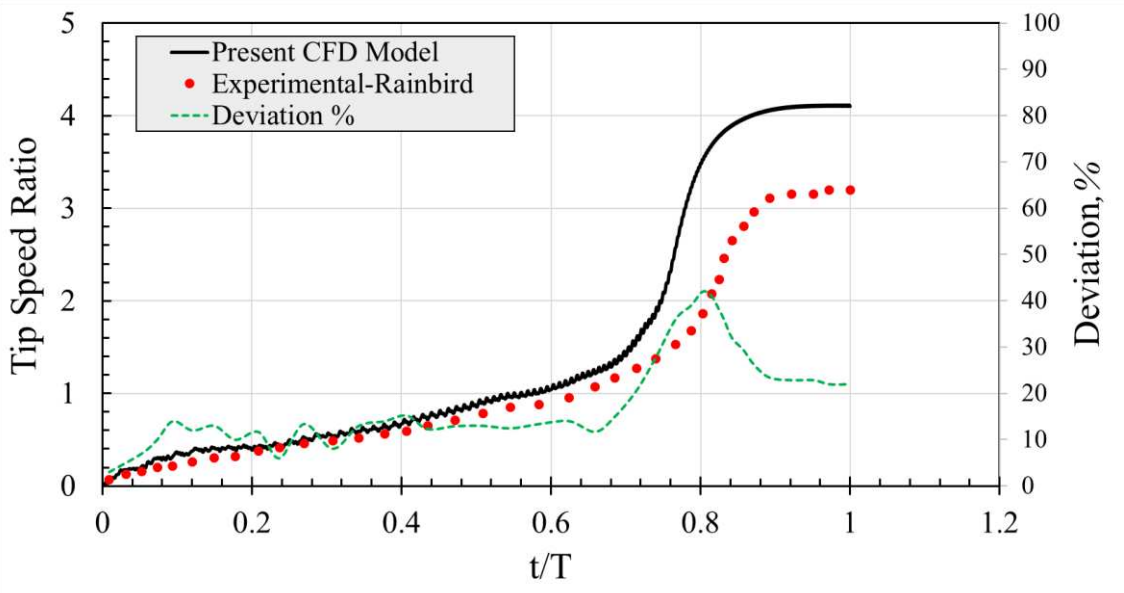

Fig. 6. The variation of the tip speed ratio as a function of the normalized time for comparison of the present CFD model with the experimental data, and deviation between CFD and experiment as a %.

As it can be seen in Fig. 6 that the turbine accelerates continuously in the experiment and reaches its steady-state condition at a TSR of about 3.2, while the CFD model result shows a similar behaviour; however, the operating TSR is about 4.1. Furthermore, the deviation between the current CFD prediction and experiment in terms of the instantaneous tip speed ratio is also presented in Fig.6. As it can be seen from the figure that in the critical tip speed ratio region, where TSR<1, the maximum deviation observed is around 16%, while the maximum discrepancy is observed to be around 40% in the acceleration region (0.7<t/T<0.82) due to a slight delay in approaching to the acceleration period.

The observed discrepancies between the experimental data and 2D CFD results could be explained to be a result of the following:

- The existence of the 3D effects, such as the blade supporting arms and tip losses, which the 2D CFD model does not take into account (Zhu et al., 2015; Castelli et al., 2011).
- Other additional sources of resistive torque, namely the bearing friction and generator losses, may result in the over-prediction of the predicted results compared to the experimental data. (Torabi et al., 2016). Because of the lack of information provided in the experimental study, the prediction of the resistive torque effect on the start-up process is not possible.
- The uncertainties related to the experimental data, such as the blade-spoke connection is not clearly mentioned in the experiment data, carried out by Rainbird (2007). The effect of the location of the blade-spoke connection on the turbine power performance (C_p) is known to be more effective at higher TSRs (Rezaeiha et al., 2018b). This may be the reason for the larger deviation of the experiment data and predicted rotational speed of the current CFD model, especially at the acceleration period and the steady state condition.
- Limitations of the numerical modelling in the prediction of the complex flows around the turbine could be a reason of the observed deviations at low TSRs, where the flow becomes more complex due to the dynamic stall.

Furthermore, a preliminary 3D CFD study has been conducted by the authors in order to compare the 3D CFD results with the current 2D CFD results and the published experimental data. The deviation between the experimental data and the present 3D result is found to be around 8.57% while it is 21.95% between the 2D and experimental data at the steady state condition. It is postulated that the difference between the 3D and experimental data may be due to the fact that additional negative torque sources such as the bearing and supporting arms, etc. have not been considered in our 3D simulations. Nevertheless, 2D simulations can still provide important insight in the fluid dynamics of self-starting process of the VAWTs, and a comprehensive 3D CFD study, which is an ongoing study by the authors, can produce a more accurate prediction of the self-starting.

In conclusion, it is very demanding to obtain a perfect match between the 2D CFD simulation results and experimental data, even in 3D, due to the limited accuracy of the numerical methods. It is postulated here that even though there is an understandable degree in the difference between the results obtained from the CFD simulations and experimental study, the behaviour of the self-starting curve of the H-type VAWT obtained from the CFD simulation is in good agreement with the curve obtained from an

experimental study. Thus, the obtained CFD model is sufficient to investigate the self-starting behaviour of the H-type VAWT.

4. Results and discussions

4.1. Aerodynamic investigation on the start-up process

It is generally believed that the Darrieus type of wind turbines are not reliable to self-start due to the weak or negative torque generation at low tip speed ratios. Fig. 7 illustrates the predicted time variation of both the moment coefficient and the tip speed ratio under constant wind speed of 6 m/s. In addition, the start-up process is divided into four zones, as indicated in Fig. 7, and a detailed investigation of these zones will be conducted in this section. As can be seen in the figure, there is only a small amount of the moment generated until TSR of 1, where the turbine acceleration is very slow. This range is generally known as the critical region.

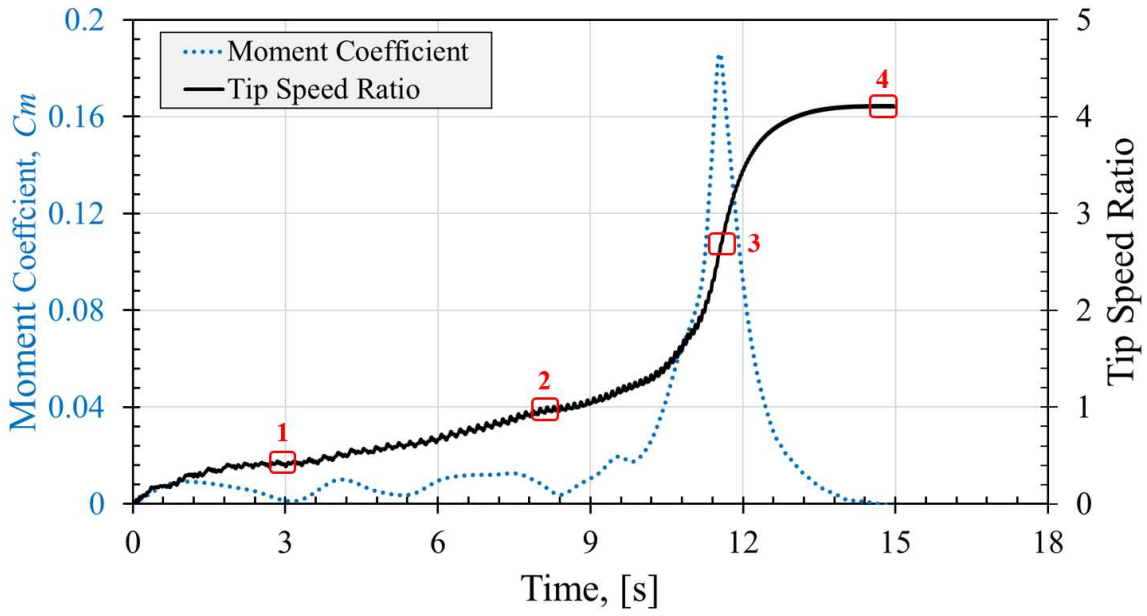

Fig. 7. Moment coefficient and tip speed ratio as a function of the time for the CFD model.

One of the ways to explain the reason of the weak self-starting behaviour of the turbine in the critical region is to plot the variations of the theoretical angle of attack as a function of the blade azimuthal angle for different tip speed ratios, as in Fig. 8. Without taking into account the effect of the induction factor, the theoretical angle of attack during the one complete revolution for different tip speed ratios can be calculated as follow (Elsakka et al., 2019);

$$AoA(\alpha) = tan^{-1}\frac{sin\theta}{TSR + cos\theta} \quad (1)$$

where θ is the blade azimuthal angle. It should be noted that there is a slight difference between the theoretical angle of attack and the effective angle of attack, however; this difference can be neglected since the induction factor does not have a significant effect on undisturbed wind velocity in the upstream part of the turbine. On the other hand, in the downstream part of the turbine, the magnitude of the effective angle of attack is smaller than the theoretical angle of attack due to the effects of several phenomena, such as stream-tube expansion, the blade-wake interaction and the flow deceleration in the front of the turbine (Elsakka et al., 2019). However, Fig. 8 helps to observe the various phenomena of the H-type VAWTs. Also, the static stall angle, where the lift coefficient achieves its maximum value, for the NACA0018 airfoil at Re = 3.5×10^4 is also marked in figure (Sheldahl and Klimas, 1981).

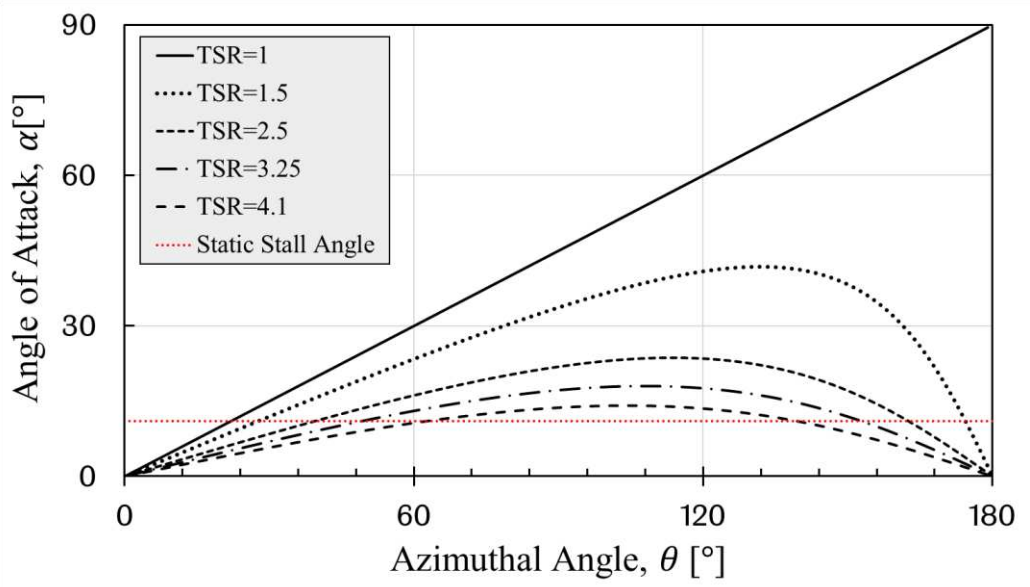

Fig. 8. Blade theoretical angle of attack as a function of the blade azimuthal angle for different TSRs.

As Fig. 8 shows that, the stall can be observed more strongly at the low tip speed ratios since the majority of the portion of the angle of attacks exceeds the static stall angle. Under these circumstances, the blade lift coefficient significantly decreases due to the large angle of attacks while the blade drag coefficient increases. Therefore, this is a crucial reason why the start-up characteristic is poor at the tip speed ratio is less than 1. However, while the tip speed ratio increases, the possibility of the stall condition decreases, which results in an improvement of the turbine torque generation and its acceleration.

In addition, to investigate the effect of lift and drag on the turbine start-up process in the critical region, the contribution of the lift and drag coefficients to the torque coefficient as a function of the blade azimuthal angle for different tip speed ratios such as 0.2, 0.4, 0.8, and 1.2 are illustrated in Fig.

9. Although the Darrieus type of VAWTs is known as lift-driven machines, the drag force might have a positive effect on the turbine start-up in the critical region. As it can be observed from the Fig. 9, when the turbine is in the critical region, where the TSR is less than 1, the turbine is not only driven by the lift. The drag also contributes to the turbine torque generation in some azimuthal angles of the complete rotor revolution; however, the contribution of the drag decreases while the tip speed ratio is approaching to 1.

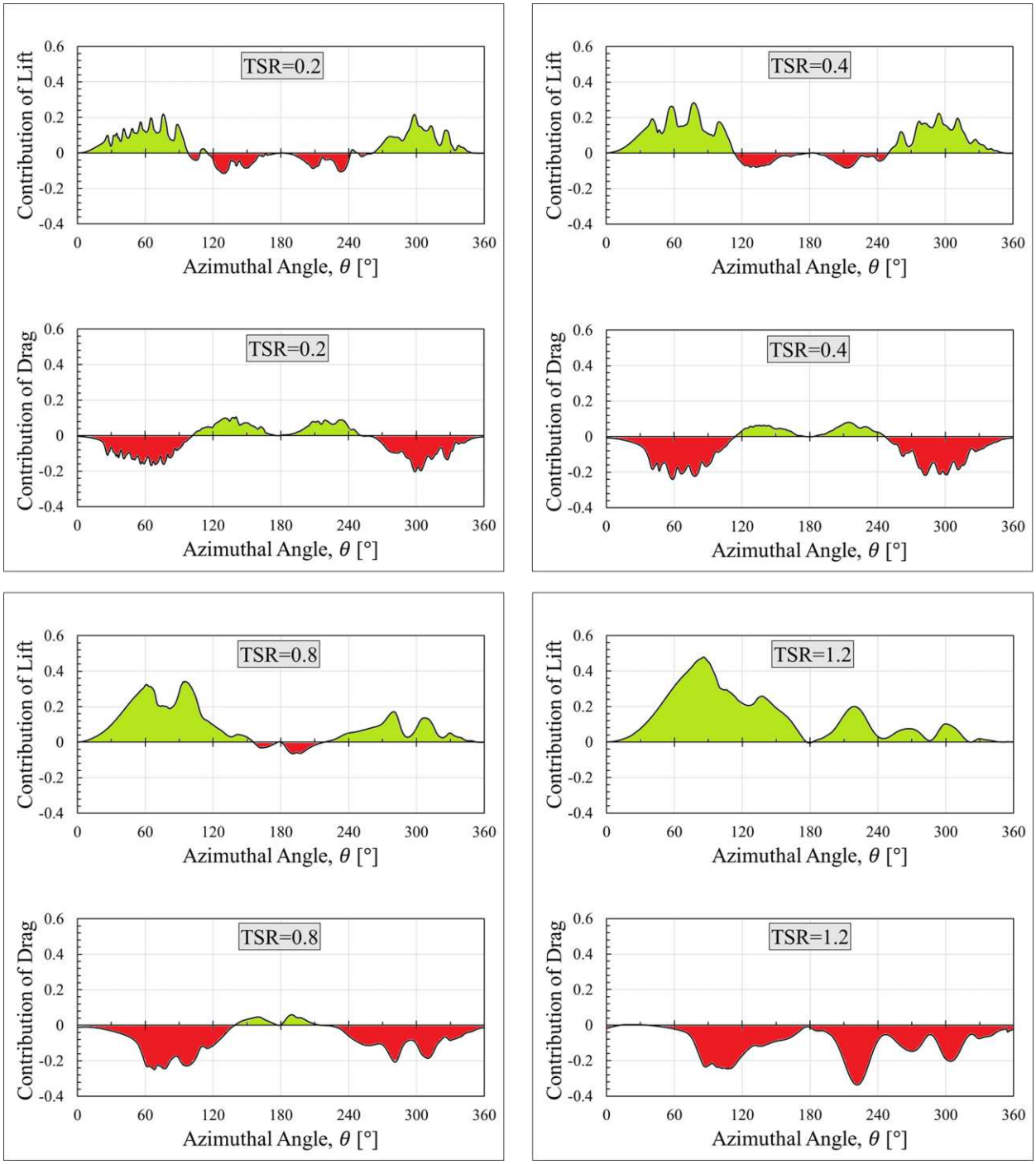

Fig. 9. The contribution of the lift and drag to the torque generation as a function of blade azimuthal angle at TSR of 0.2, 0.4, 0.8, and 1.2.

It can also be observed in the figure that when the tip speed ratio is less than 1; the region of the positive lift contribution is more significant than the negative drag contribution, while the region of the positive drag contribution is more significant than the negative lift contribution in a complete rotor revolution. This situation leads to a positive average torque generation, which results in the increasing of the self-starting capability of the turbine. In addition, the average turbine torque coefficients as a function of the tip speed ratios are illustrated in Fig. 10. Although the turbine might generate negative instantaneous torque coefficient in some azimuthal angles in a complete rotor revolution, (see Fig. 9), the all average torque coefficients are positive and increases with increasing the tip speed ratio, as shown in Fig. 10, which makes the turbine speed up.

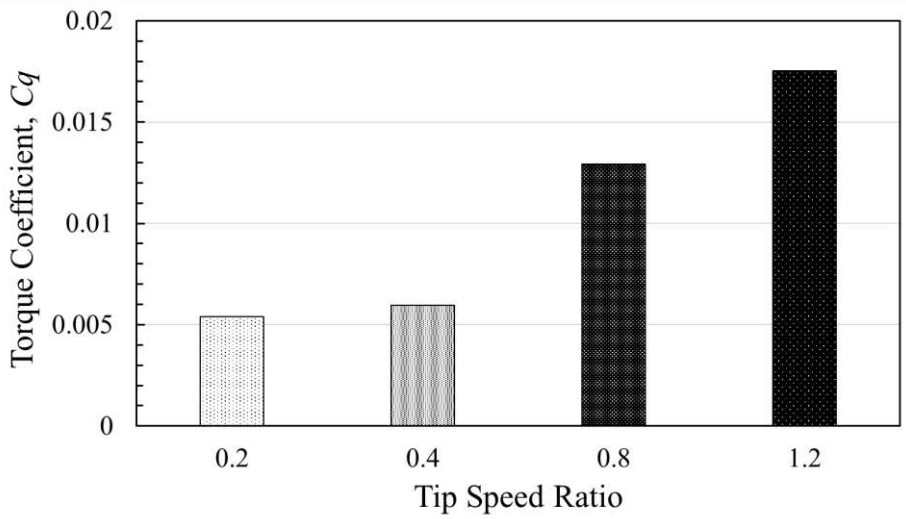

Fig. 10. The turbine torque coefficient as a function of the different tip speed ratios, such as 0.2, 0.4, 0.8, and 1.2.

It should be also noted that, as stated above, the magnitude of the effective angle of attack, especially in the downstream part of the turbine, is smaller than the theoretical angle of attack. Therefore, according to the study (Rezaeiha et al., 2018b), the measured AoA at the downstream part of turbine is almost halved compared to the theoretical value at high tip speed ratios, and based on this assumption, the contribution of the lift and drag to the turbine torque generation has been calculated for the TSRs of 0.4 and 0.8. The deviation between the theoretical AoA and effective AoA in the contribution of the lift and drag to the total torque is found to be less than 5% and the difference is expected to be even less at reduced TSRs. Therefore the calculated lift and drag contributions to the torque generation based on the real angle of attack, which is not always readily available for the downstream part, is found to be only a little different from that based on the theoretical AoA in the turbine self-starting investigation.

To investigate the self-starting process of Darrieus type of VAWT in detail, the self-starting curve as shown in Fig. 6 may be divided into zones, which are Zone 1, Zone 2, Zone 3, and Zone 4 indicated as the red squares in Fig. 7. These four TSR zones have been selected corresponding to the TSR values,

0.5, 1, 2.57, and 4.1. Fig. 11 shows the turbine moment coefficients as a function of the blade azimuthal angles in the four zones. As it can be seen in the figure, at low TSR regions, such as Zone 1 and Zone 2, the complexity of the moment coefficient curve is due to the fact that in some azimuthal positions of a complete rotor revolution, the direction of the net aerodynamic forces acting on the blade is contrary to the direction to the turbine rotation, which results in a negative or weak net force generation. The reason behind this situation is that the drag force overcomes the lift force, which results in an instantaneous negative torque generation. Even though the instantaneous torque is negative in a certain azimuthal position, the average torque at each tip speed ratio is positive, which may increase the possibility of the self-stating of the turbine, and this aggress with the findings discussed by Beri and Yao, (2011). As the turbine rotational speed increases up to Zone 3, the average turbine moment coefficient reaches its maximum value, and the moment coefficient curve becomes smoother. On the other hand, in Zone 4, the turbine reaches its steady-state position, where the average moment coefficient becomes almost zero, due to the balance between the generated positive lift and negative drag forces.

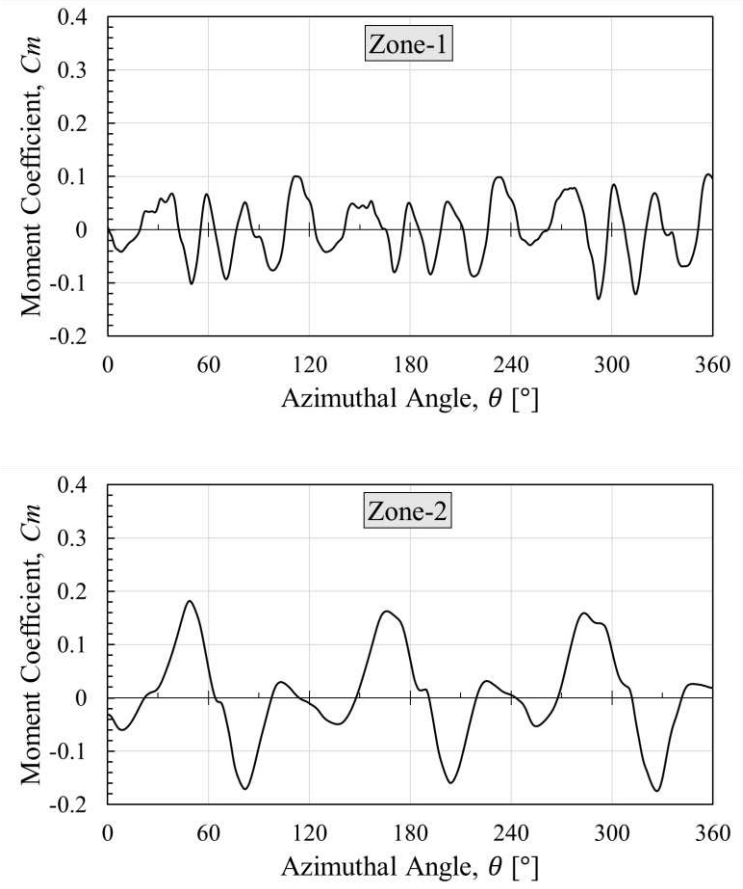

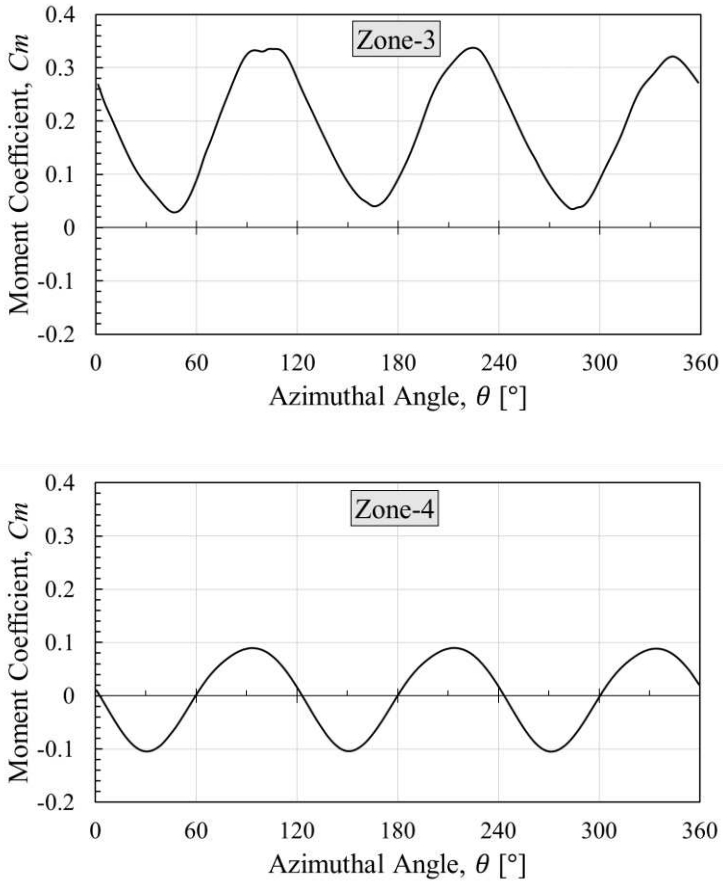

Fig. 11. Turbine moment coefficients as a function of the blade azimuthal angle in the four zones.

For further analyses, the visualisation of the flow around the airfoils is shown in Fig. 13, which compares the non-dimensional vorticity contours for each zone at azimuthal angles of 0°, 60°, 120°, and 180°. At low TSR regions, such as Zone 1 and Zone 2, each blade experiences high and low angles of attack, which causes a complex flow pattern. The existence of these complex vorticities in Zone 1 and Zone 2 leads to a slower, or even no starting of the turbine, which may be mainly due to the lower lift force of the blade. When the tip speed ratio is greater than 1, the blade vortices become smaller, and the blades generate a higher lift force. For this reason, the turbine acceleration increases considerably, and this can be seen in Fig. 7 between 9s and 14s. After 14s, although no separation occurs (Zone 4), the low angles of the attack reduces the maximum possible lift force on the blades. In addition, another situation may cause the reduction in the turbine performance in Zone 4, which is the blades increase the pressure in the front of the turbine and the turbine reacts like a solid wall, and there is a significant amount of the wind that passes around the turbine. In order to clarify this situation, the non-dimensional velocity magnitude contours for the turbine in Zone 1 and Zone 4 have been presented in Fig. 12. As it can be seen in the figure that, the amount of the wind passing towards to the downstream part of the turbine in Zone 4 is less than in Zone 1 due to the high pressure in the front of the turbine. This condition

is called the blockage effect, which reduces the lift force generation in the downstream part of the turbine and overall turbine efficiency.

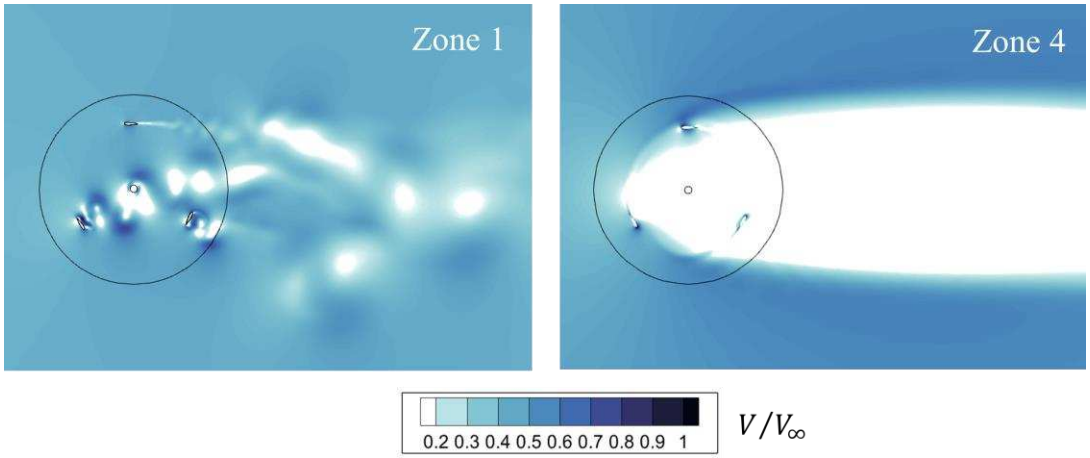

Fig. 12. Dimensionless velocity magnitude around the blades for Zone 1 and Zone 4.

Eventually, it can be understood that one of the most critical parameters for the turbine to accelerate to a steady-state condition may be the gradually eliminating of the initial complex vorticities. The reduction in the complex patterns can be observed in the non-dimensional vorticity contours from Zone 1 to Zone 4, see Fig. 13.

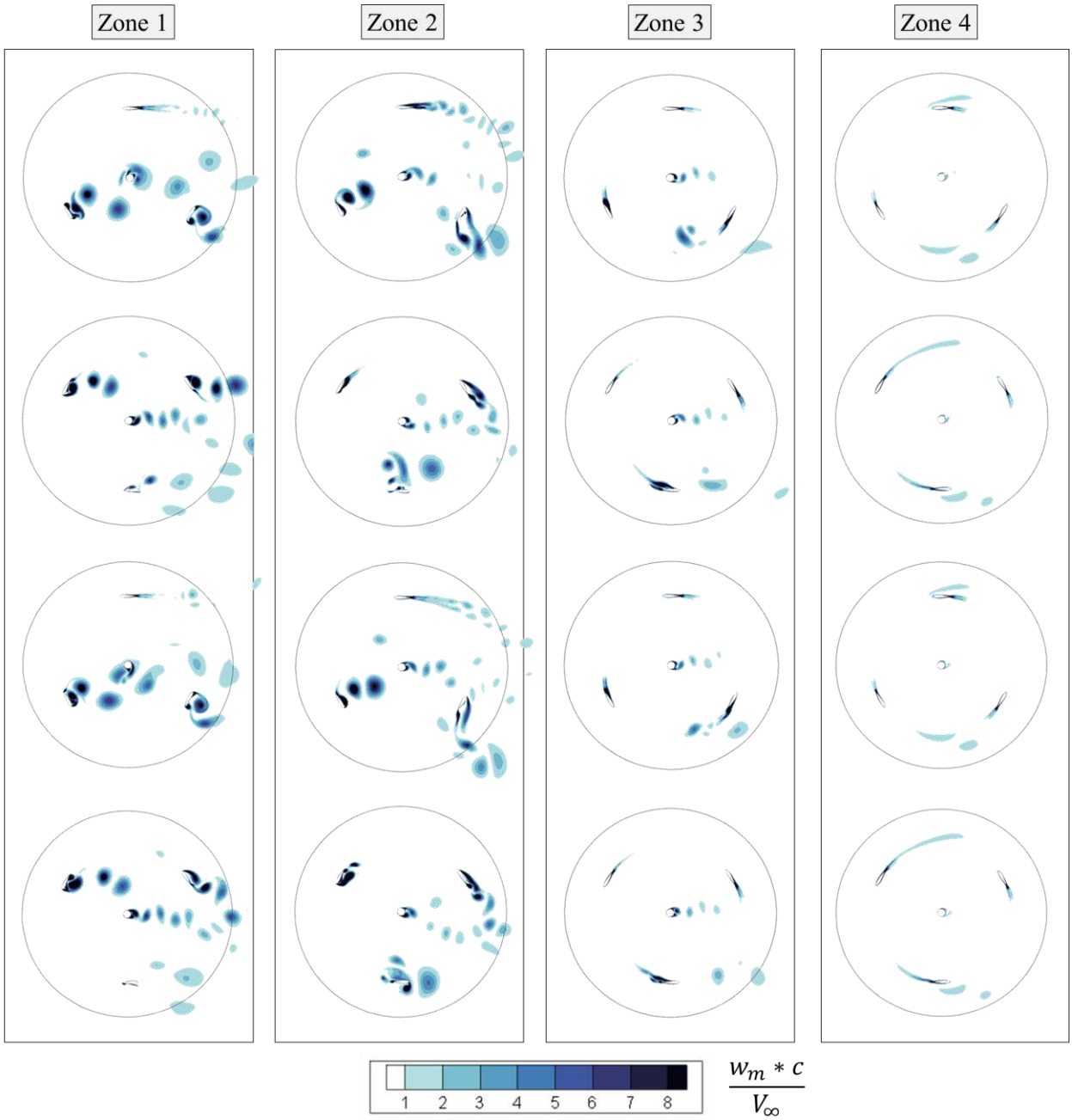

Fig. 13. Non-dimensional vorticity contours around the blades for the four zones at 60° intervals of the azimuthal angle.

As a summary of the H-type of VAWT start-up process, the variation of tip speed ratio as a function of the normalised time is illustrated in Fig. 14. What is interesting in this figure that H-type VAWTs operate in two different conditions during the start-up process, such as a combined stage, which is lift-drag driven, and fully lift driven stage. The turbine in the combined stage, where the turbine is driven by lift and drag, proceeds until the TSR=1. In this region, the positive drag contribution plays a significant role in the second and third quarter of the rotor revolution, where the azimuthal position varies between 100° and 253°, as shown in Fig. 14. Once the TSR>1, the turbine enters the fully lift-driven stage.

Overall, these findings indicate that the main driving force of the turbine in the critical region is both lift and drag forces. Therefore, in order to improve the self-starting capability of the H-type VAWT in the critical region, not only the lift force but also the drag force at the position, where the drag force assists the turbine rotating motion, should be increased. Additionally, when the TSR≥1, the lift-driven is required to be maintained in order to achieve a complete start-up process.

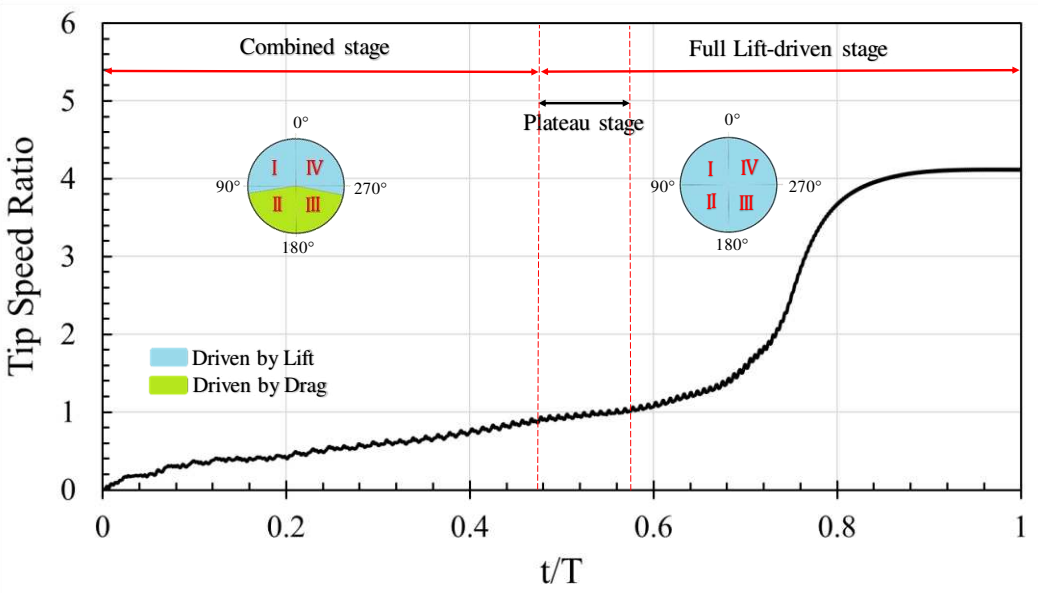

Fig. 14. The variation of the tip speed ratio as a function of the normalised time to show the summary for the H-type VAWT start-up process.

4.2. Moment of inertia effect on the self-starting and performance of the turbine

In this part of the study, four different moments of inertia of the turbine, namely Inertia 1, Inertia 2, Inertia 3, and Inertia 4, which have the inertia values as $0.0105\ kgm^2$, $0.0211\ kgm^2$, $0.03\ kgm^2$, and $0.0422\ kgm^2$, respectively, have been selected to investigate the inertia effect on self-starting behaviour and turbine performance. Inertia 3 has been selected as the base case, where the mass of the blade is the same as in the experiment condition, and other mass values have been selected proportionally.

As stated above, the turbine starts rotating from rest and accelerates until its steady-state condition is reached, where the turbine rotational speed is oscillating around the same average value. Fig. 15 shows the effects of different turbine moments of inertia on the turbine acceleration as a function of the non-dimensional time. It can be observed from the figure that increasing the turbine moment of inertia from $0.0105\ kgm^2$ to $0.0422\ kgm^2$, extends the time required to reach its steady-state condition.

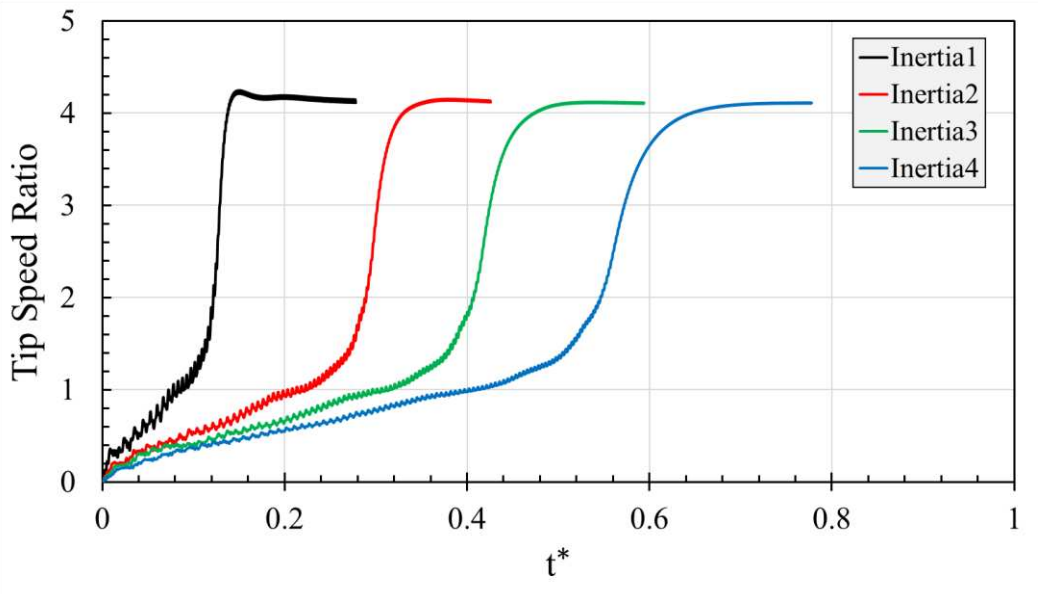

Fig. 15. The tip speed ratio as a function of the non-dimensional time for different moments of inertia.

It is observed from this figure that even though the moment of inertia is changed, the average value of the turbine rotational speed at the steady-state condition is the same for all investigated inertia cases. The turbine moment of inertia effect at its steady-state condition is illustrated in Fig. 16, and it can be observed that as the turbine moment of inertia increases, the amplitude of fluctuation of the turbine rotational speed decreases. Furthermore, from the data in Fig. 16, it is apparent that if the moment of inertia is doubled, the amplitude of the oscillation is about halved; e.g., h2 is half of the h1.

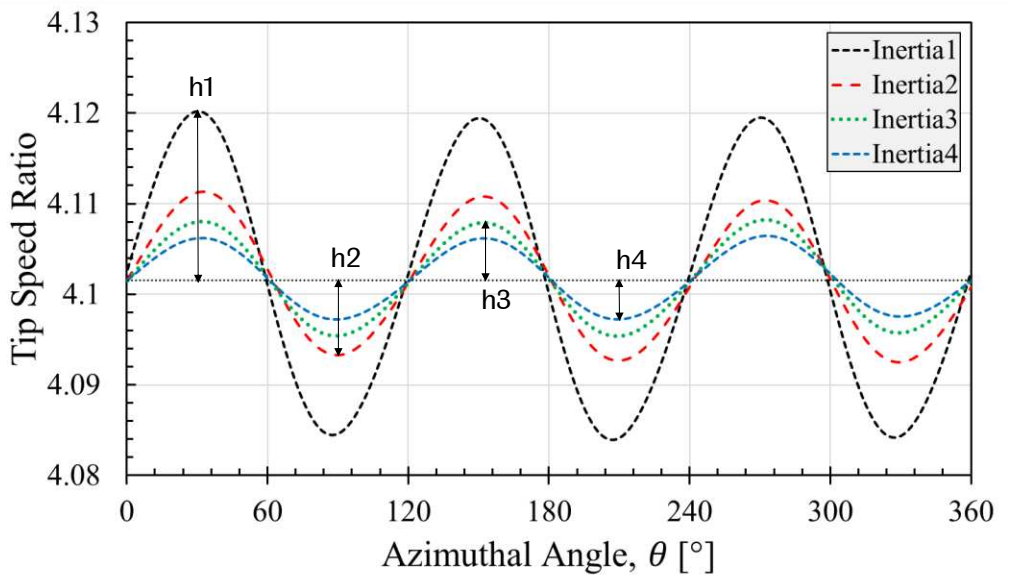

Fig. 16. The TSR as a function of the blade azimuthal angle for the four inertias at the final steady-state condition.

In order to discuss the effect of the inertia on the performance of the turbine, the turbine power coefficient as a function of the tip speed ratio curve during the start-up process is plotted in Fig. 17. It should be noted that the values of the power coefficients and the tip speed ratios have been averaged in one revolution of the turbine. Therefore, each point in the Cp/TSR curve indicates one complete revolution for each inertia case. It can be observed in the figure that the four inertias produce a similar value for the power coefficients until the tip speed ratio reaches 2.6, where the turbine has passed the plateau stage and has started up as shown in Fig. 7. After this point, the lighter turbine shows a higher instantaneous performance until the final steady tip speed ratio reached, as illustrated in Fig. 17 in the TSRs marked as A, B, and C.

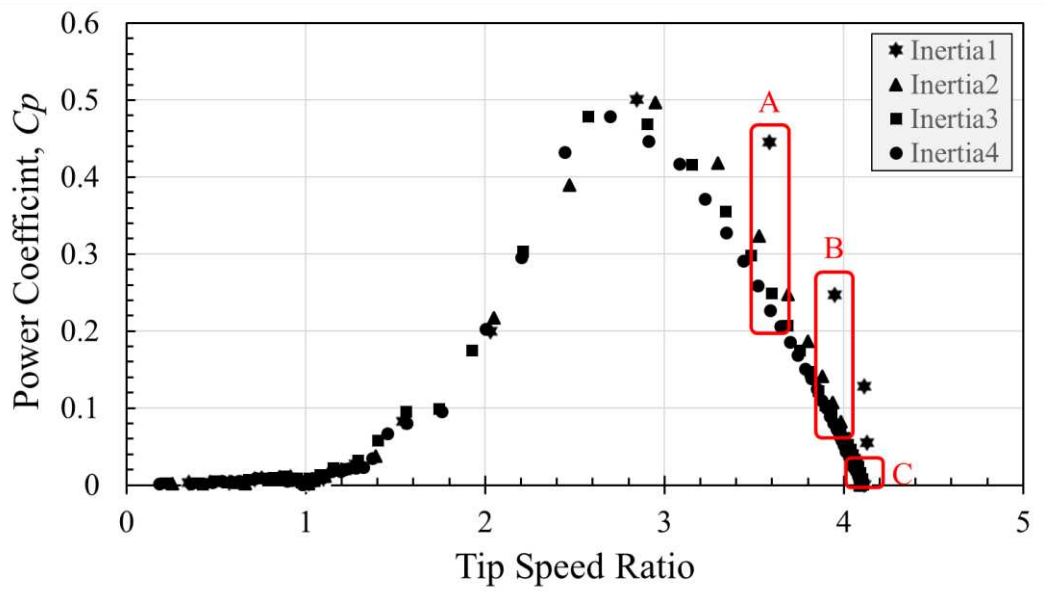

Fig. 17. The power coefficient as a function of the TSR for the four inertias investigated.

To investigate the aerodynamic behaviour of the lighter turbine and compare it with other turbines after TSR of 2.6, the blade moment coefficients as a function of the azimuthal angle for Zone A, Zone B, and Zone C as indicated in Fig. 17 are illustrated in Fig. 18. It can be seen in the figures that in Zone A and Zone B, the blade instantaneous moment coefficient of the Inertia 1, especially in the upstream part of the turbine, is higher than the other turbines, which results in a higher power coefficient in these regions. In Zone C, the instantaneous moment coefficients of all inertia cases show similar behaviour and this is due to the turbine reaching steady-state conditions.

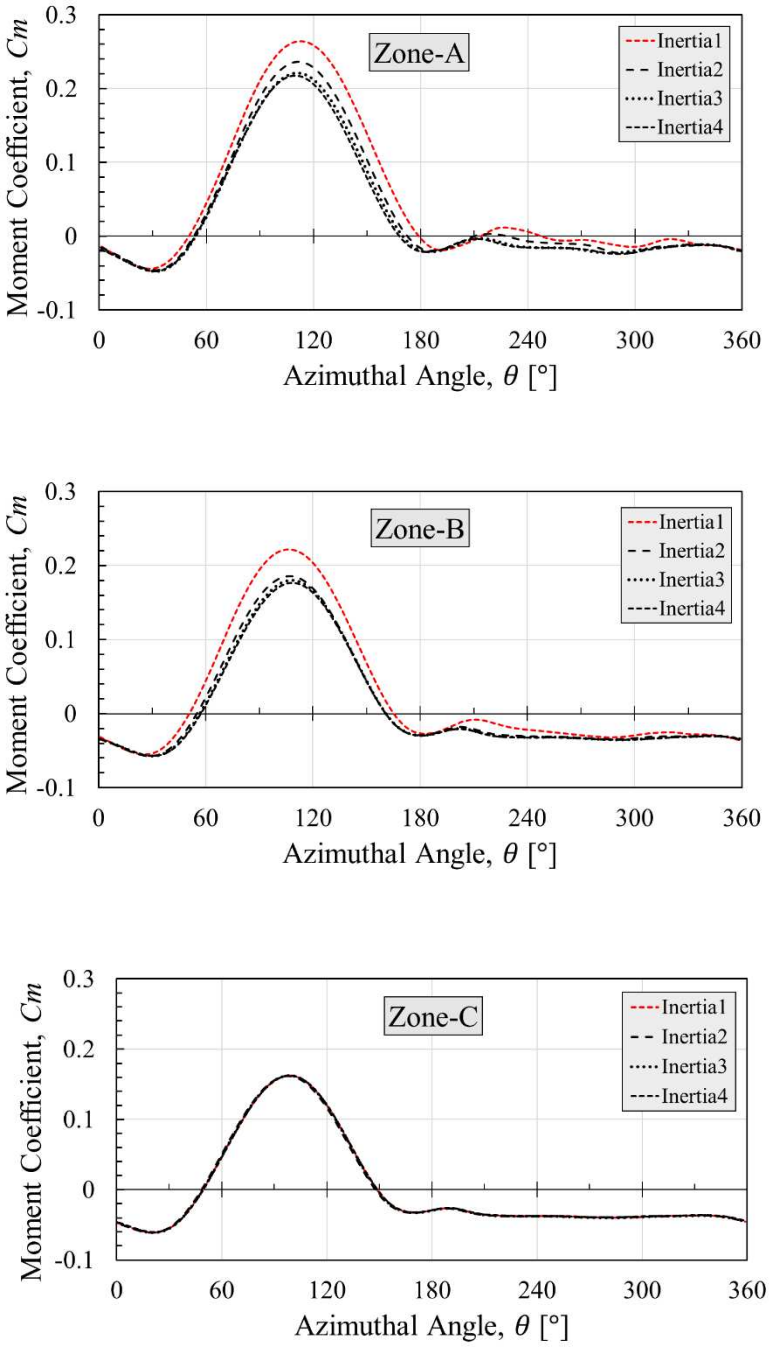

Fig. 18. The moment coefficient as a function of azimuthal angle for Zone A, Zone B, and Zone C.

In addition, the lift and drag coefficient of the four inertia cases in Zone A are plotted in Fig. 19 and it can be observed that the lighter turbine produces the higher lift coefficient and lower drag coefficient in this region, which may result in the higher power coefficient. Although the higher drag coefficient contributes to the starting torque at low tip speed ratios, it decreases the turbine performance at high tip speed ratios, as explained in the previous section.

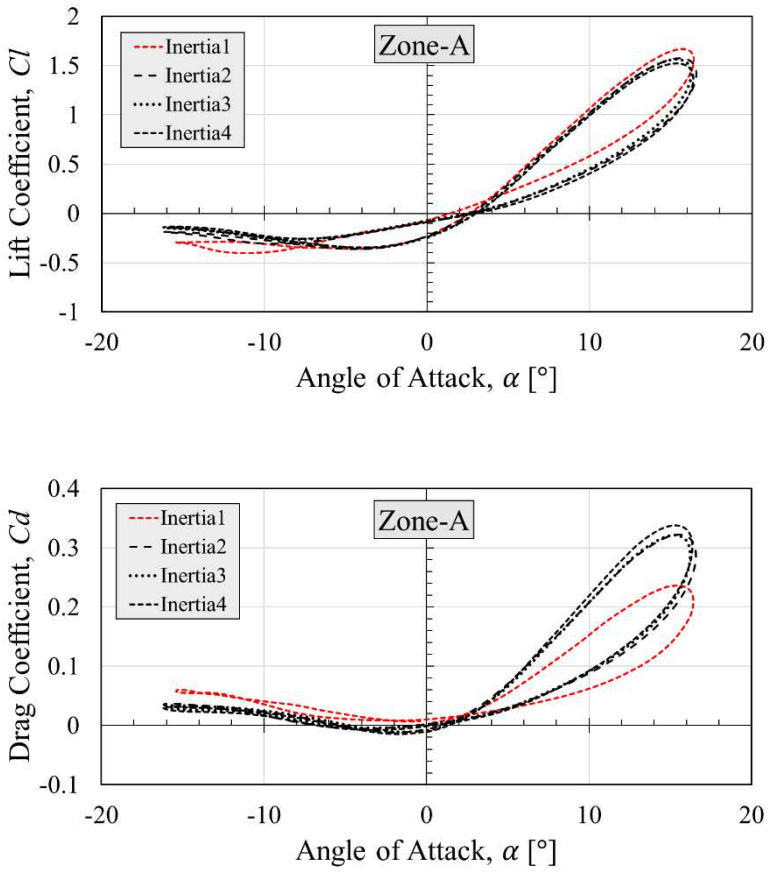

Fig. 19. The lift and drag coefficient as a function of angle of attack for Zone A.

Furthermore, investigating the acceleration rates of the four inertia cases may help to understand the reason for the higher power coefficient of the lighter turbine. Therefore, the variation of the tip speed ratio as a function of the normalised time is plotted for the four inertia cases in Fig. 20 (a). It is apparent from the figure that the tip speed ratios of all inertia cases increase similarly until the point 1, where the tip speed ratio is around 2.6, and then the discrepancy became more obvious until the point 2, where deceleration starts before the steady-state condition. Between the point 1 and 2, the lighter turbine has a higher acceleration rate compared to other turbines, as can be seen in the enlarged view (Fig.20 (b)). Therefore, it is believed that the reason for the higher lift and lower drag coefficients of the lighter turbine, which results in higher power coefficient, might be due to this acceleration rate. However, further experimental investigations are recommended in order to confirm the findings.

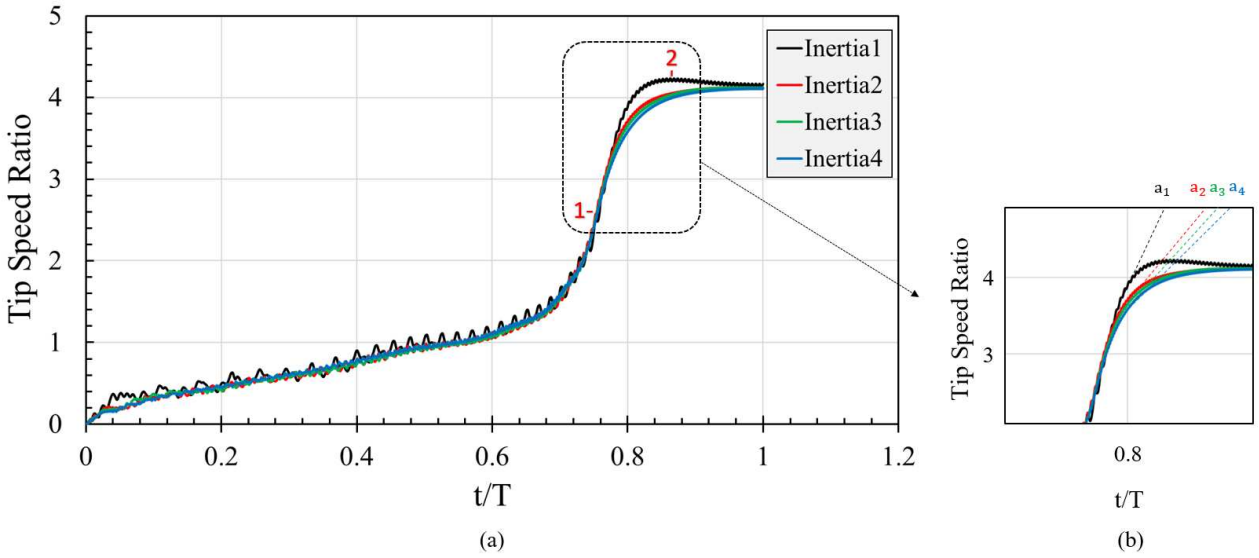

Fig. 20. (a) The tip speed ratio as a function of the non-dimensional time axis for inertia cases and (b) its enlarged view.

In conclusion, increasing the moment of inertia of the turbine increases the time to reach the final rotational speed. However, it did not show a noticeable effect on the starting of the turbine and the final speed. In addition, the TRS range is the same in all the cases investigated, and the lighter turbine has a higher power coefficient after the peak power coefficient has been reached. Although the lighter turbine shows a better performance after the optimum TSR, the amplitude of oscillation of the rotational speed, which is in direct proportion to the torque, is increased during the start-up process (see Fig. 15 and Fig.16). As a result, the vibration and fatigue stress acting on the turbine may increase (Zamani et al., 2016). For this reason, optimum inertia could be determined in order to achieve quick turbine start-up while reducing the vibration and fatigue issues.

4.3. The effect of the blade number on both self-starting and performance of the turbine

The blade number is one of the important parameters affecting the turbine start-up performance of the H-type VAWTs, conforming to the turbine solidity. In this study, the turbine solidity is determined as a ratio between the area of the blades and turbine radius, and simply defined as follow:

$$Solidity\ (\sigma) = \frac{N_b \times c}{R} \tag{2}$$

where N_b is the number of blades, c is the chord length of the blade, and R is the radius of the turbine. In order to investigate the effect of the blade number on the self-starting behaviour and performance of the H-type VAWT with NACA0018 blade profile, the blade numbers of the turbine are changed as 2, 3, 4, and 5 while the chord length and the radius of the turbine are kept constant. Turbine self-

starting, time-varying data is presented for 2, 3, 4, and 5-bladed turbines in order to observe the number of blade effect on turbine start-up behaviour

Fig. 21 shows the variation of the tip speed ratio as a function of the time for the investigated turbines. As it can be seen in the figure that the 2-bladed turbine fails to self-start; however, the times required to reach the steady-state condition are 15s, 11s, and 9.5s, when the numbers of blades are N=3, 4, and 5, respectively.

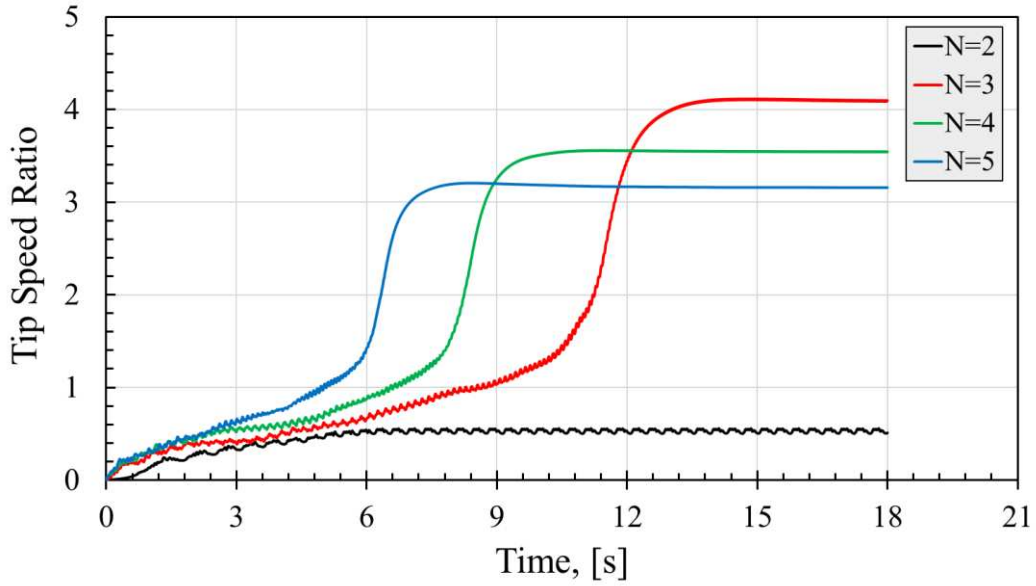

Fig. 21. The variation of the tip speed ratio as a function of the time for 2, 3, 4, and 5-bladed turbines.

In order to assess the start-up behaviour and the performance of an H-type VAWT, three essential parameters, such as the start-up time, the peak power coefficient, and the optimum tip speed ratio, where the peak power coefficient is obtained, should be considered. Generally, shorter start-up time and a higher peak power coefficient at a higher optimum tip speed ratio are required in order to achieve optimum performance of an H-type VAWT. Therefore, the optimum tip speed ratio, the peak power coefficient, and the start-up time of H-type VAWT as a function of the different number of blades are illustrated in Fig. 22. The optimum tip speed ratios are 2.57, 2.31, and 2.1, when the numbers of blades are N=3, 4, and 5, respectively. On the other hand, the peak power coefficient can be obtained as 0.478, 0.432, and 0.398, when the numbers of blades are N=3, 4, and 5, respectively. The findings in this part of the study are subjected to three important phenomena. First, the optimum tip speed ratio decreases with the increase of the number of blades. Second, the start-up time decreases with the increase of the number of blades. Third, the peak power coefficient also decreases with the increase of the number of blades. It should be noted that the information of the 2-bladed turbine does not exist in the Fig. 22 due to the fact that it does not show the self-starting characteristics.

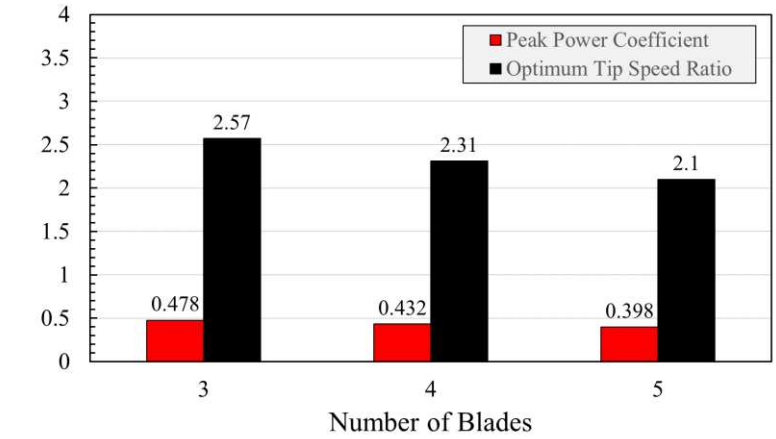

Fig. 22. Aerodynamic characteristics of the H-type VAWT with the different number of blades: (a) optimum tip speed ratio and peak power coefficient, (b) start-up time.

Furthermore, the turbine power coefficient in the low tip speed ratio region (0<TSR<1) has been calculated and plotted in Fig.23. From this figure, it is noted that the values of the power coefficients and tip speed ratios have been averaged over one complete revolution of the turbine from the dynamic start-up simulations. In addition, the 2-bladed turbine is not included in Fig. 23 since it does not show any self-starting characteristics. Fig. 23 also illustrates that the larger is the number of blades then a slightly higher power coefficient at low tip speed ratios is obtained, which increases the self-starting capability of the turbine. This observed finding in the current study appears to be consistent with other researches (Rezaeiha et al., (2018b); Li et al., (2015).

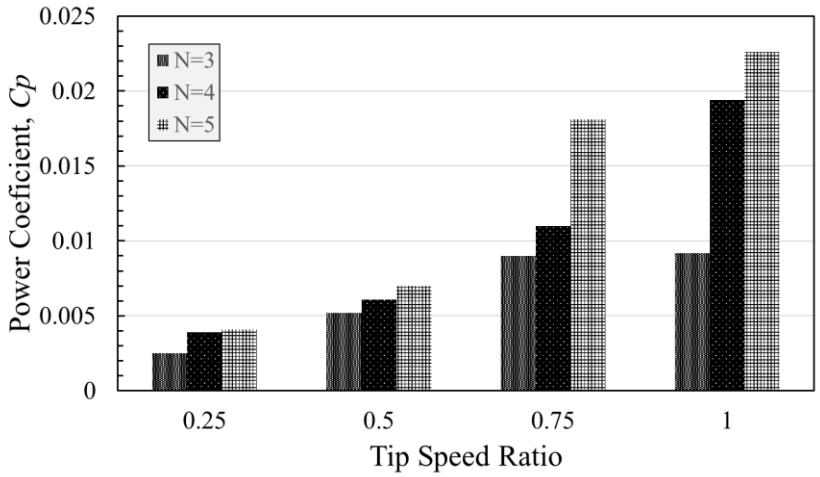

Fig. 23. Turbine power coefficient as a function of the tip speed ratio for different number of blades.

Consequently, the good self-starting performance of the H-type VAWTs can be determined by a quick start-up time and a peak power coefficient at an optimum tip speed ratio. For the turbines studied in this paper, the peak power coefficient is achieved when the number of blades is 3; however, the quicker time to reach steady-state condition is achieved when the number of blades is 5. Therefore, it is apparent that the blade number cannot make the turbine having both larger power coefficient and quicker start-up time. According to the CFD start-up simulation results, it can be argued that the optimum turbine performance might be obtained with 3 blades in terms of the start-up time and peak power coefficient.

Conclusions

In the present study, a CFD self-starting model has been employed in order to evaluate the self-starting behaviour of the H-type vertical axis wind turbines. The predicted behaviour of the self-starting of the H-type VAWT obtained from the CFD simulation is in good agreement with the curve obtained from the experimental data. The important findings of the present study are as follows:

- In the critical region (TSR<1), the positive drag contributes to the torque generation in the second and third quarters of the rotor revolution, where the range of the azimuthal angles vary between 100° and 253°. Once TSR>1, the turbine enters a stage where the turbine is fully driven by the lift force.
- In order to improve the self-starting capability of the H-type VAWT in the critical region, not only the lift force but also the drag force at the position, where the drag force assists the turbine rotating motion, should be enhanced.

- When the TSR≥1, the lift-driven is required to be maintained in order to achieve a complete start-up process.
- Increasing the moment of inertia of the turbine increases the time to reach the final rotational speed. However, it does not show a noticeable effect on the starting of the turbine and the final speed.
- An instantaneous increase in the power efficiency is observed during the start-up process when the turbine escapes from the plateau stage due to an increase in the acceleration rate of the lighter turbine.
- The peak power coefficient is achieved when the number of blades is 3; however, a faster start-up time is achieved when the number of blades is 5. Therefore, a compromise between the start-up and the power efficiency may have to be made in the design of the turbine.
- The larger number of blades allows the reaching of a slightly higher power coefficient at low tip speed ratios (TSR<1), which increases the self-starting capability of the turbine.

The limitations of the study are as follows:

- In order to improve the accuracy of the model, the additional resistive torque sources, such as the bearing friction and generator losses, should be considered in the rotational speed calculation. However, due to the lack of information provided in the experimental investigations, the prediction of the resistive torque effect on the start-up process is not possible.
- 3D simulations are required to consider 3D effects, in such as the blade supporting arms and tip losses, which the 2D CFD model does not take into account.
- The contribution of the lift and drag coefficients to the turbine torque generation at the low tip speed ratios has been calculated based on the theoretical angle of attack. However, in order to achieve more precise results, the effective angle of attack should be considered in the calculations.

Acknowledgement

Yunus Celik would like to thank the Ministry of National Education of Turkey for their financial support during his PhD studies.

Nomenclature

a	Acceleration Rate (rad/s^2)
a	Angle of Attack
c	Chord length (m)
Cm	Moment Coefficient
Cp	Power Coefficient
Cq	Torque Coefficient
I	Moment of Inertia (kgm^2)
y^+	Dimensionless wall distance
ω	Rotational speed (rad/s)
σ	Solidity
$t*$	Non-dimensional time
w_m	Vorticity magnitude ($1/s$)
V_∞	Free wind speed (m/s)
V	Velocity magnitude (m/s)

Abbreviations

AoA	Angle of Attack
BEM	Blade Element Momentum
CFD	Computational Fluid Dynamics
HAWT	Horizontal Axis Wind Turbine
Re	Reynolds Number
RNG	Re-Normalisation Group
SST	Shear Stress Transport
TSR	Tip Speed Ratio
VAWT	Vertical Axis Wind Turbine

References

Almohammadi, K.M., 2014. Optimization of a CFD Based Design of a Straight blade Vertical Axis Wind Turbine (SB-VAWT). The University of Leeds, PhD thesis,.

ANSYS, 2013. ANSYS Fluent User's Guide Release 15.0. Canonsburg: ANSYS Inc.

ANSYS Inc., 2014. Introduction to Ansys Fluent-Turbulence Modeling.

Balduzzi, F., Bianchini, A., Maleci, R., Ferrara, G., Ferrari, L., 2016. Critical issues in the CFD simulation of Darrieus wind turbines. Renew. Energy 85, 419–435.

Bedon, G., De Betta, S., Benini, E., 2015. A computational assessment of the aerodynamic performance of a tilted Darrieus wind turbine. J. Wind Eng. Ind. Aerodyn. 145, 263–269.

Beri, H., Yao, Y., 2011. Numerical Simulation of Unsteady Flow to Show Self-starting of Vertical Axis Wind Turbine Using Fluent. J. Appl. Sci. 962–970.

BerténYi, T., Wickins, C., McIntosh, S., 2010. Enhanced Energy Capture Through Gust-Tracking in the Urban Wind Environment. 48th AIAA Aerosp. Sci. Meet. Incl. New Horizons Forum Aerosp. Expo. 1376.

Bhuyan, S., Biswas, A., 2014. Investigations on self-starting and performance characteristics of simple H and hybrid H-Savonius vertical axis wind rotors. Energy Convers. Manag. 87, 859–867.

Bos, R., 2012. Self-starting of a small urban Darrieus rotor. Strategies to boost performance in low-reynolds-number flows. Delft University of Technology, Master of Science Thesis.

Castelli, M.R., Ardizzon, G., Battisti, L., Benini, E., Pavesi, G., 2010. Modeling Strategy and Numerical Validation. Proc. ASME 2010 Int. Mech. Eng. Congr. Expo. 1–10.

D'Alencon, J.P., Silva-Llanca, L., 2016. Two-dimensional numerical analysis of a low-re turbulent impinging synthetic jet. Proc. 15th Intersoc. Conf. Therm. Thermomechanical Phenom. Electron. Syst. ITherm 2016 921–929.

Douak, M., Aouachria, Z., Rabehi, R., Allam, N., 2018. Wind energy systems: Analysis of the self-starting physics of vertical axis wind turbine. Renew. Sustain. Energy Rev. 81, 1602–1610.

Ebert, P.R., Wood, D.H., 1997. Observations of the starting behavior of a small horizontal- axis wind turbine. Renew. Energy 12, 245–257.

Edwards, J.M., Angelo Danao, L., Howell, R.J., 2012. Novel experimental power curve determination and computational methods for the performance analysis of vertical axis wind turbines. J. Sol. Energy Eng. Trans. ASME 134, 1–11.

Elsakka, M.M., Ingham, D.B., Ma, L., Pourkashanian, M., 2019. CFD analysis of the angle of attack for a vertical axis wind turbine blade. Energy Convers. Manag. 182, 154–165.

Hosseini, A., Goudarzi, N., 2019. Design and CFD study of a hybrid vertical-axis wind turbine by employing a combined Bach-type and H-Darrieus rotor systems. Energy Convers. Manag. 189, 49–59.

Juneja, S.K., Sobti, N., Wais, A., 2012. Solar Energy: A Clean Energy System, International Conference on Renewable Energy for Institutes and Communities in Urban and Rural Settings.

Kaya, M.N., Kose, F., Ingham, D., Ma, L., Pourkashanian, M., 2018. Aerodynamic performance of a horizontal axis wind turbine with forward and backward swept blades. J. Wind Eng. Ind. Aerodyn. 176, 166–173.

Kirke Brian, 1988. Evaluation of Self-Starting Vertical Axis Wind Turbines for Stand-Alone Applications. Griffith University, Australia.

Kose, F., Kaya, M.N., 2013. Analysis on meeting the electric energy demand of an active plant with a wind-hydro hybrid power station in Konya, Turkey: Konya water treatment plant. Renew. Energy 55, 196–201.

Langtry, R.B., Menter, F.R., Likki, S.R., Suzen, Y.B., Huang, P.G., Völker, S., 2006. A correlation-based transition model using local variables - Part II: Test cases and industrial applications. J. Turbomach. 128, 423–434.

Li, Q., Maeda, T., Kamada, Y., Hiromori, Y., Nakai, A., Kasuya, T., 2017. Study on stall behavior of a straight-bladed vertical axis wind turbine with numerical and experimental investigations. J. Wind Eng. Ind. Aerodyn. 164, 1–12.

Li, Q., Maeda, T., Kamada, Y., Murata, J., Furukawa, K., Yamamoto, M., 2015. Effect of number of blades on aerodynamic forces on a straight-bladed Vertical Axis Wind Turbine. Energy 90, 784–795.

Liu, K., Yu, M., Zhu, W., 2019. Enhancing wind energy harvesting performance of vertical axis wind turbines with a new hybrid design: A fluid-structure interaction study. Renew. Energy 140, 912–927.

Lunt, P.A.V., 2005. An aerodynamic model for a vertical-axis wind turbine. MEng project report,School of Engineering, University of Durham, UK.

Menter, F.R., 2009. Review of the shear-stress transport turbulence model experience from an industrial perspective. Int. J. Comut. Fluid Dyn. 23, 305–316.

Menter, F.R., 1994. Two-equation eddy-viscosity turbulence models for engineering applications. AIAA J. 32, 1598–1605.

Menter, F.R., Langtry, R., Vollker, S., Huang, P.G., 2005. Transition Modelling for General Purpose CFD Codes. Eng. Turbul. Model. Exp. 6 31–48.

Nahas, M.N., 1993. A self-starting darrieus-type windmill. Energy 18, 899–906.

Nobile, Rosario, Vahdati, M., Barlow, J.F., Mewburn-Crook, A., 2014. Unsteady flow simulation of a vertical axis augmented wind turbine: A two-dimensional study. J. Wind Eng. Ind. Aerodyn. 125, 168–179.

Posa, A., 2020. Influence of Tip Speed Ratio on wake features of a Vertical Axis Wind Turbine. J. Wind Eng. Ind. Aerodyn. 197, 104076. 6

Raciti Castelli, M., Englaro, A., Benini, E., 2011. The Darrieus wind turbine: Proposal for a new performance prediction model based on CFD. Energy 36, 4919–4934.

Rainbird, J., 2007. The aerodynamic development of a vertical axis wind turbine. MEng Proj. ReporSchool Eng. Univ. Durham, UK.

Rezaeiha, A., Kalkman, I., Blocken, B., 2017. CFD simulation of a vertical axis wind turbine operating at a moderate tip speed ratio: Guidelines for minimum domain size and azimuthal increment. Renew. Energy 107, 373–385.

Rezaeiha, A., Montazeri, H., Blocken, B., 2018a. Towards accurate CFD simulations of vertical axis wind turbines at different tip speed ratios and solidities: Guidelines for azimuthal increment, domain size and convergence. Energy Convers. Manag. 156, 301–316.

Rezaeiha, A., Montazeri, H., Blocken, B., 2018b. Characterization of aerodynamic performance of vertical axis wind turbines: Impact of operational parameters. Energy Convers. Manag. 169, 45–77.

Rezaeiha, A., Montazeri, H., Blocken, B., 2018c. Towards optimal aerodynamic design of vertical axis wind turbines: Impact of solidity and number of blades. Energy 165, 1129–1148.

Roache, P.J., 1997. Quantification of Uncertainty in Computational Fluid Dynamics. Annu. Rev. Fluid Mech. 29, 123–160. https://doi.org/10.1146/annurev.fluid.29.1.123

Rossetti, A., Pavesi, G., 2013. Comparison of different numerical approaches to the study of the H-Darrieus turbines start-up. Renew. Energy 50, 7–19.

Sengupta, A.R., Biswas, A., Gupta, R., 2016. Studies of some high solidity symmetrical and unsymmetrical blade H-Darrieus rotors with respect to starting characteristics, dynamic performances and flow physics in low wind streams. Renew. Energy 93, 536–547.

Sheldahl, R.E., Klimas, P.C., 1981. Aerodynamic characteristics of seven symmetrical airfoil sections through 180-degree angle of attack for use in aerodynamic analysis of vertical axis wind turbines.

Singh, M.A., Biswas, A., Misra, R.D., 2015. Investigation of self-starting and high rotor solidity on the performance of a three S1210 blade H-type Darrieus rotor. Renew. Energy 76, 381–387.

Song, C., Zheng, Y., Zhao, Z., Zhang, Y., Li, C., Jiang, H., 2015. Investigation of meshing strategies and turbulence models of computational fluid dynamics simulations of vertical axis wind turbines. J.

Renew. Sustain. Energy 7.

Sun, X., Zhu, J., Hanif, A., Li, Z., Sun, G., 2020. Effects of blade shape and its corresponding moment of inertia on self-starting and power extraction performance of the novel bowl-shaped floating straight-bladed vertical axis wind turbine. Sustain. Energy Technol. Assessments 38, 100648.

Torabi, M., Zal, E., Mustapha, F., Wiriadidjaja, S., 2016. Study on start-up characteristics of H-Darrieus vertical axis wind turbines comprising NACA 4-digit series blade airfoils. Energy 112, 528–537.

Untaroiu, A., Wood, H.G., Allaire, P.E., Ribando, R.J., 2011. Investigation of Self-Starting Capability of Vertical Axis Wind Turbines Using a Computational Fluid Dynamics Approach. J. Sol. Energy Eng. 133, 041010.

Wekesa, D.W., Wang, C., Wei, Y., Zhu, W., 2016. Experimental and numerical study of turbulence effect on aerodynamic performance of a small-scale vertical axis wind turbine. J. Wind Eng. Ind. Aerodyn. 157, 1–14.

Worasinchai, S., Ingram, G.L., Dominy, R.G., 2012. The Physics of H-Darrieus Turbines Self-Starting Capability: Flapping-Wing Perspective. Proc. ASME Turbo Expo 2012.

Zamani, M., Maghrebi, M.J., Varedi, S.R., 2016. Starting torque improvement using J-shaped straight-bladed Darrieus vertical axis wind turbine by means of numerical simulation. Renew. Energy 95, 109–126. https://doi.org/10.1016/j.renene.2016.03.069

Zhang, L.X., Liang, Y.B., Liu, X.H., Jiao, Q.F., Guo, J., 2013. Aerodynamic performance prediction of straight-bladed vertical axis wind turbine based on CFD. Adv. Mech. Eng. 2013.

Zhu, J., Huang, H., Shen, H., 2015. Self-starting aerodynamics analysis of vertical axis wind turbine. Adv. Mech. Eng. 7, 1–12.

Zhu, J. yang, Jiang, L., Zhao, H., 2016. Effect of wind fluctuating on self-starting aerodynamics characteristics of VAWT. J. Cent. South Univ. 23, 2075–2082.